Elucidation and optimization of the interaction of nanostructured DNA and immune cells

2017

Shozo OHTSUKI

Contents

Preface

Nucleic acids are the key molecules of signal transduction in humans and other organisms. Genetic information is stored in the genomic DNA, and vital activity is constantly carried out through RNA transcribed as necessary. In recent years, research on nucleic acid drugs has progressed rapidly. Various classes of nucleic acid drugs are currently used or under development[1,2], and some nucleic acid-based drugs have been approved for clinical use[3]. The negative charge of nucleotide backbone greatly limits the cellular uptake of nucleic acid-based drugs. To overcome this limitation, many chemical modifications on these nucleic acid-based drugs are applied to increase their nuclease resistance and cellular uptake by target cells[4–6].

Unmethylated cytosine-phosphate-guanine dinucleotide with appropriate flanking sequences, or CpG motif, is a pathogen-associated molecular pattern and a ligand for Toll-like receptor 9 (TLR9) expressed in various mammalian immune cells[7–9]. The binding of CpG DNA, a DNA containing the CpG motif, to the receptor leads to the production of proinflammatory cytokines, including tumor necrosis factor (TNF)-α, interleukin (IL)-6, and interferon (IFN)-α[10,11]. Therefore, CpG DNA has attracted attention in the treatment of cancer, virus infection, and allergic diseases[12–16]. However, CpG DNA has not been clinically applied yet.

DNA has a unique property to hybridize with its complementary sequence. More recently, DNA nanotechnology has greatly increased the potential of DNA as a building block for DNA assemblies. So far, some unique structures have been developed using DNA[17–21]. These DNA structures could be used as therapeutic agents or drug delivery systems. My laboratory reported that multi-branched, polypod-like structured DNA, or polypodna, prepared using three or more oligodeoxynucleotides (ODNs), is a useful DNA nanostructure for the delivery of natural phosphodiester CpG DNA to mouse macrophage-like RAW264.7 cells, mouse dendritic DC2.4 cells, mouse bone marrow-derived dendritic cells, and human peripheral blood mononuclear cells[22–25]. The polypod-like structure was found to be quite effective for the delivery of DNA to these immune cells.

However, there is little information about the interaction of nanostructured DNA and target cells. Therefore, I aimed to develop efficient delivery systems to immune cells using nanostructured DNA. To achieve this, the interaction of nanostructured DNA and immune cells needs to be elucidated and optimized. In Chapter I, I elucidated the structural properties of nanostructured DNA that are required for the interaction with immune cells. In Chapter II, I focused on the effect of the structural rigidity or structural compactness of nanostructured DNA on the interaction with immune cells using DNA origami or DNA supramolecules. Finally, in Chapter III, I elucidated cell surface receptors that are involved in the cellular uptake of nanostructured DNA.

In this thesis, the results are presented in the following three chapters.

Chapter I

Elucidation of the structural properties of nanostructured DNA required for the interaction with immune cells

Recent advances in DNA nanotechnology have greatly increased the potential of DNA strands as a building block for DNA assemblies[26]. A variety of uniquely structured DNA assemblies, such as DNA origami-based nanostructures[17], DNA polyhedral[18], and DNA hydrogel[20,27], have been reported. Some of these have been examined as pharmaceuticals or drug delivery systems[26,28].

My laboratory previously demonstrated that nanostructure formation increased CpG DNA-induced immune activation[22–25,29]. However, detailed studies on the interaction of nanostructured DNA with cells are needed to develop nanostructured DNA-based delivery systems for efficient delivery of nucleic acid drugs including CpG DNA to target cells.

In this chapter, I aimed to elucidate the structure-activity relationship of self-assembled nanostructured DNA as delivery vehicles for target cells. I designed three different nanostructured DNAs using four 55-mer oligodeoxynucleotides (ODNs), that is tetrapod-like structured DNA (tetrapodna), tetrahedral DNA (tetrahedron), and tetragonal DNA (tetragon), and compared their potencies. These three nanostructured DNAs were compared in terms of preparation efficiency, physicochemical property, and interaction with the cells. Additionally, I hypothesized bend type DNA could be efficiently taken up by immune cells. Moreover, for clinical use, it is necessary to evaluate the cellular uptake of nanostructured DNAs by cells other than target cells. Therefore, I selected tripodna, terapodna, hexapodna, terahedron, and tetragon to examine their uptake in several types of cells.

In this chapter, the results are presented in the following three sections.

Chapter I

Section 1

Optimal arrangement of four short DNA strands for delivery of immunostimulatory nucleic acids to immune cells

I-1-1 Introduction

Apart from the use of chemically stabilized DNA/RNA analogues, such as phosphorothioate DNA[30,31], several attempts have been made to increase the activity of natural phosphodiester CpG DNA through efficient delivery of the DNA to the target immune cells. Separately, Li et al. reported that DNA tetrahedron, designed using four ODNs, was useful for the delivery of CpG DNA to RAW264.7 cells[32]. These previous studies have clearly demonstrated that nanosized DNA assemblies are suitable systems for the delivery of CpG DNA to immune cells for immunostimulation. However, no systematic studies have been carried out to elucidate the optimal structure of such DNA assemblies for the delivery of immunostimulatory CpG DNA to immune cells.

In this section, I examined the importance of the structure of nanosized DNA assemblies in the preparation efficiency as well as the stimulation of immune cells. Since previous study from my laboratory demonstrated that the number and length of ODNs were key parameters for the physicochemical and biological properties of polypodnas[24], these parameters were fixed in order to extract the structure-dependent differences among the nanosized DNA assemblies. To this end, tetrahedral DNA (tetrahedron) consisting of four 55-mer ODNs, reported by Li et al.[32], was selected as one of the DNA assemblies for comparison. To minimize the difference in the sequences, one of the ODNs for the tetrahedron (the common ODN) was used to newly design tetrapodna consisting of four 55-mer ODNs. In addition, a tetragonal DNA (tetragon) was also designed with the common ODN and three other 55-mer ODNs. These three DNA nanostructures were compared in terms of preparation efficiency, physicochemical property, cellular uptake, and immunostimulatory activity. RAW264.7 cells and human peripheral blood mononuclear cells (PBMCs) were used for cellular interaction of these DNA nanostructures.

I-1-2 Materials and Methods

Chemicals

Roswell Park Memorial Institute (RPMI) 1640 medium was obtained from Nissui Pharmaceutical, Co., Ltd. (Tokyo, Japan). Opti-MEM was purchased from Life Technologies (Rockville, MD, USA). Fetal bovine serum (FBS) was obtained from HyClone Laboratories, Inc. (South Logan, UT, USA). The 100 base pair (bp) DNA ladder was purchased from Takara Bio (Otsu, Japan). All other chemicals were the highest grade available and used without further purification.

Cell culture

The murine macrophage-like cell line RAW264.7 was cultured in RPMI medium supplemented with 10% heat-inactivated FBS, 0.2% sodium bicarbonate, 100 IU/mL penicillin, 100 μg/mL streptomycin, and 2 mM L-glutamine at 37°C in humidified air containing 5% CO_2. RAW264.7 cells were then plated on 24-well or 96-well culture plates at a density of 5×10^5 cells/mL and cultured for 24 h prior to use.

Isolation of human peripheral blood mononuclear cells

All experiments using human primary cells were approved by the institutional review board at the Graduate School of Medicine, Kyoto University, and following the tenets of the Declaration of Helsinki. Human PBMCs were obtained from healthy donors after obtaining their written informed consent. PBMCs were isolated from peripheral blood by density gradient centrifugation using Lympholyte-H Cell Separation Media (Cedarlane Laboratories Ltd., Netherlands) as previously reported[33]. Cells collected were replated on 48-well culture plates at a density of 6×10^5 cells/well in RPMI medium.

Oligodeoxynucleotides

All ODNs used were purchased from Integrated DNA Technologies, Inc. (Coralville, IA, USA). The sequences of the ODNs used are listed in Table 1. ODN-1-1-1 was the common ODN used for all three preparations. Each ODN, such as tetrapodna-1-1-2, tetrahedron-1-1-2, and so on, was identified with the name of the DNA assembly and the ODN number. For cellular uptake experiments, ODN-1-1-1 labeled with Alexa Fluor-488 at the 5′ end (Alexa ODN-1-1-1) was purchased from Japan BioService Co., Ltd. (Saitama, Japan). CpG ODN-1 was designed in such a way that a 25-base ODN containing a potent CpG motif was linked to the 5′-end of the ODN-1-1-1, and used for cytokine release experiments. AFM-tetrapodna-1-1-1, AFM-tetrapodna-1-1-3, AFM-tetrahedron-1-1-2, AFM-tetrahedron-1-1-3, AFM-tetragon-1-1-2, and AFM-tetragon-1-1-3 were used for AFM imaging.

Preparation of DNA nanostructures

ODNs dissolved in an annealing buffer (TE buffer; 10 mM Tris-HCl, pH 8, 1 mM ethylenediaminetetraacetic acid (EDTA), and 50 mM magnesium chloride) were mixed at a final concentration of 0.5–20 μM for each ODN. The annealing buffer was used to prepare all the DNA samples. The mixtures were then incubated at 95°C for 2 min and slowly cooled down to 4°C using a thermal cycler. The annealing condition for tetrahedron was optimized in preliminary experiments, and a different condition from the original one[32] was used to minimize the formation of aggregates at high DNA concentrations. Each preparation was analyzed at 37°C by the MCE-202 MultiNA microchip electrophoresis system for DNA/RNA analysis (Shimadzu, Kyoto, Japan) or

by 6% polyacrylamide gel electrophoresis. Double-stranded (ds) DNA was prepared by annealing of ODN-1-1-1 and ODN-1-1-1′.

Atomic force microscopy imaging of DNA nanostructures

Atomic force microscopy (AFM) images were obtained on a high-speed AFM system (Nano Live Vision, RIBM, Tsukuba, Japan) using a silicon nitride cantilever (BL-AC10EGS; Olympus, Tokyo, Japan) as reported previously[34]. All the DNA nanostructures were immobilized to the DNA frame using the two long single-stranded sequences on the 5′-end of the two ODNs of each DNA nanostructure. In brief, a DNA sample was adsorbed on a freshly cleaved mica plate pretreated with 0.1% aqueous 3-aminopropyltriethoxysilane for 5 min at room temperature and then washed three times with a buffer solution containing 20 mM Tris and 10 mM $MgCl_2$. Scanning was performed in the same buffer solution.

Measurement of melting temperature

The melting temperatures (Tm) were obtained by measuring the absorbance of tetrapodna, tetrahedron, and tetragon in TE buffer containing 50 mM $MgCl_2$ at 260 nm with a Shimadzu UV-1600 PC spectrometer (Shimadzu, Kyoto, Japan) equipped with a TMSPC-8 temperature controller[29].

Dynamic light scattering analysis

The apparent sizes of tetrapodna, tetrahedron, and tetragon were determined by the dynamic light scattering method using a Malvern Zetasizer 3000HS (Malvern Instruments, Malvern, UK) at 20°C. The measurement was repeated more than eight times, and the results were expressed as the mean ± SD of the eight measurements.

Circular dichroism spectra of DNA nanostructures

The circular dichroism (CD) spectra of DNA were recorded using a JASCO-820 type spectropolarimeter (JASCO, Tokyo, Japan) with a 0.1 cm path-length quartz cell at 20°C. The DNA samples after annealing were diluted with 50 mM $MgCl_2$-containing TE buffer to a final DNA concentration of 68 μg/mL. The CD spectra of DNA were measured in the range of 200 to 320 nm.

Stability of DNA nanostructures in 50% FBS

DNA nanostructures (68 μg/mL) were mixed with non-heat-inactivated FBS of equal volume and incubated at 37°C. After 0, 2, 4, 8, 12, or 24 h of incubation, a 10 μL aliquot of the sample solution was transferred to plastic tubes and mixed with 20 μL of 0.5 M EDTA solution to stop the degradation, and then stored at -20°C until use. These samples were run on 9% polyacrylamide gel electrophoresis (PAGE) at 4°C and stained with SYBR Gold (Life Technologies). The density of the DNA bands was quantitatively evaluated using the Multi Gauge software (Fujifilm, Tokyo, Japan).

Cellular uptake of DNA

RAW264.7 cells or PBMCs on 96 or 48-well plates at a density of 5×10^4 or 6×10^5 cells/well were incubated with Alexa Fluor 488-labeled single-stranded DNA (ssDNA), tetrapodna, tetrahedron, or tetragon diluted in 0.1 mL of Opti-MEM for 2 or 4 h at 37°C. Cells were then washed three times with 200 or 400 μL of phosphate-buffered saline and harvested. Then, the fluorescent intensity of cells was determined by flow cytometry (FACS Calibur or Gallios Flow Cytometer, BD Biosciences, NJ, USA) using CellQuest software (version 3.1, BD Biosciences) or Kaluza software (version 1.0, BD Biosciences), and the mean fluorescence intensity (MFI) was calculated.

TNF-α release from RAW264.7 cells

RAW264.7 cells were seeded into 96-well plates at a density of 5×10^4 cells/well. Then, CpG ssDNA, CpG tetrapodna, CpG tetrahedron, or CpG tetragon was diluted in 0.1 mL of Opti-MEM and added to the cells. The cells were incubated at 37°C for 8 h, and the supernatants were retrieved and stored at -80°C until use. The levels of TNF-α in the supernatants were determined by enzyme-linked immunosorbent assay (ELISA) using OptEIA™ sets (BD Biosciences).

IFN-α release from human PBMCs

PBMCs were seeded into 48-well plates at a density of 6×10^5 cells/well. Then, CpG ssDNA, CpG tetrapodna, CpG tetrahedron, or CpG tetragon was diluted in 0.2 mL of Opti-MEM and added to the cells. The cells were incubated at 37°C for 24 h, and the supernatants were retrieved and stored at -80°C until use. The levels of human IFN-α were determined using the IFN-α–ELISA module set (Bender Med Systems, Vienna, Austria). Chloroquine (Sigma-Aldrich, St. Louis, MO, USA) was used as a control for TLR involvement PBMCs. Cells were incubated with or without 100 μM chloroquine.

Statistical analysis

Differences were statistically evaluated by one-way analysis of variance (ANOVA) followed by the Tukey-Kramer test for multiple comparisons. A P value of <0.05 was considered statistically significant.

Table 1. The sequences of ODNs for DNA nanostructures.

Name	Sequences (5′ → 3′)	Length (mer)
ODN-1-1-1	ACATTCCTAAGTCTGAAACATTACAGCTTGCTACACGAGAAGAGCCGCCATAGTA	55
Alexa ODN-1-1-1	*ACATTCCTAAGTCTGAAACATTACAGCTTGCTACACGAGAAGAGCCGCCATAGTA	55
ODN-1-1-1′	TACTATGGCGGCTCTTCTCGTGTAGCAAGCTGTAATGTTTCAGACTTAGGAATGT	55
tetrapodna-1-1-2	TTACTATGGCGGCTCTTCTCGTGTAGCATAGTGTCGTTTTATCACCAGGCAGTTG	55
tetrapodna-1-1-3	TCAACTGCCTGGTGATAAAACGACACTACGTGGGAATCTTGACAGGTCATCAGCC	55
tetrapodna-1-1-4	TGGCTGATGACCTGTCAAGATTCCCACGAGCTGTAATGTTTCAGACTTAGGAATG	55
tetrahedron-1-1-2	TATCACCAGGCAGTTGACAGTGTAGCAAGCTGTAATAGATGCGAGGGTCCAATAC	55
tetrahedron-1-1-3	TCAACTGCCTGGTGATAAAACGACACTACGTGGGAATCTACTATGGCGGCTCTTC	55
tetrahedron-1-1-4	TTCAGACTTAGGAATGTGCTTCCCACGTAGTGTCGTTTGTATTGGACCCTCGCAT	55
tetragon-1-1-2	CTGTAATGTTTCAGACTTAGGAATGTTTTGAAGTGACGCCAGAGTAGATTCCCAC	55
tetragon-1-1-3	GTGTCGTTTTATCACCAGGCAGTTGATTTTACTATGGCGGCTCTTCTCGTGTAGC	55
tetragon-1-1-4	TCAACTGCCTGGTGATAAAACGACACTTTGTGGGAATCTACTCTGGCGTCACTTC	55
CpG ODN-1-1-1	TCCAT**GACGTT**CCTGACGTTTTTTTACATTCCTAAGTCTGAAACATTACAGCTTGCTACACGAGAAGAGCCGCCATAGTA	80
AFM-tetrapodna-1-1-1	ATAAGAATAAACACCGCATCATTATAACATTCCTAAGTCTGAAACATTACAGCTTGCTACACGAGAAGAGCCGCCATAGTA	81
AFM-tetrapodna-1-1-3	CGAGCTGAAAAGGTGGCATCATTATATCAACTGCCTGGTGATAAAACGACACTACGTGGGAATCTTGACAGGTCATCAGCC	81

AFM-tetrahedron-1-1-2	ATAAGAATAAACACCGCATCATTATACATCATCATCATGCTCAATATCACCAGGCAGTTGACAGTGTAGCAAGCTGTAATAGATGCGAGGGTCCAATAC	99
AFM-tetrahedron-1-1-3	CGAGCTGAAAAGGTGGCATCATTATACATCATTGTATGACTATATCAACTGCCTGGTGATAAAACGACACTACGTGGGAATCTACTATGGCGGCTCTTC	99
AFM-tetragon-1-1-2	ATAAGAATAAACACCGCATCATTATACATCATCATCATGCTCTGTAATGTTTCAGACTTAGGAATGTTTTGAAGTGACGCCAGAGTAGATTCCCAC	96
AFM-tetragon-1-1-3	CGAGCTGAAAAGGTGGCATCATTATACATCATTGTATGACTGTGTCGTTTTATCACCAGGCAGTTGATTTTACTATGGCGGCTCTTCTCGTGTAGC	96

All ODNs have a phosphodiester backbone. The asterisk (*) indicates the position of Alexa Fluor-488 modification. Underlined is the CpG motif (GACGTT).

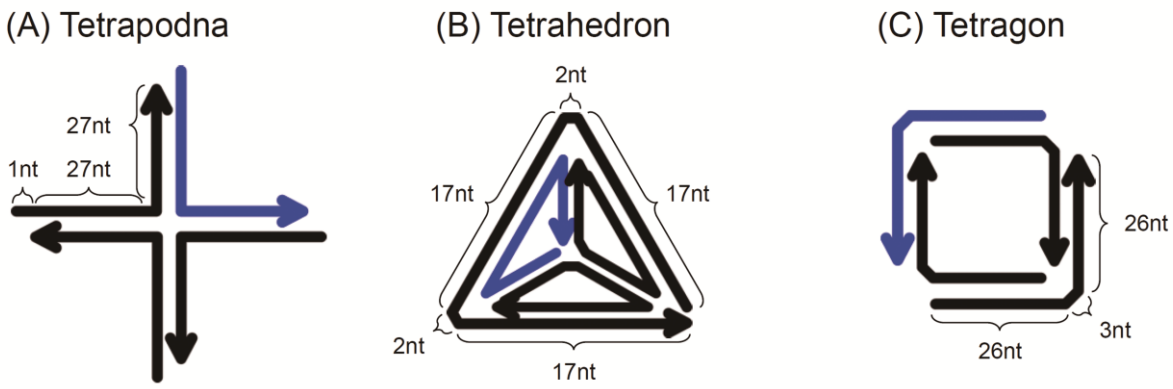

Figure 1. Schematic presentation of tetrapodna, tetrahedron, and tetragon. The blue-colored arrows are the common ODN (ODN1-1-1). The arrowheads represent the 3′-end of each ODN.

I-1-3 Results

I-1-3-a. Construction of DNA nanostructures

Figure 1 shows the schematic images of tetrapodna, tetrahedron, and tetragon. The blue-colored lines indicate the common ODN (ODN-1-1-1) for all preparations. Figure 2A shows the MultiNA analysis of tetrapodna, tetrahedron, and tetragon prepared at various DNA concentrations (0.5–20 μM). A fixed amount of DNA (68 ng) was run on electrophoresis. Tetrapodna had a major single band of around 140 bp at all the DNA concentrations examined (Figure 2A, lanes 1–5), indicating that tetrapodna was successfully formed with high efficiency by simple annealing of ODNs. On the other hand, the band for tetrahedron, which was detected around 90 bp, became weaker with increasing DNA concentrations at preparation (Figure 2A, lanes 6–10). There were several bands for tetragon prepared at high DNA concentrations (Figure 2A, lanes 11–15).

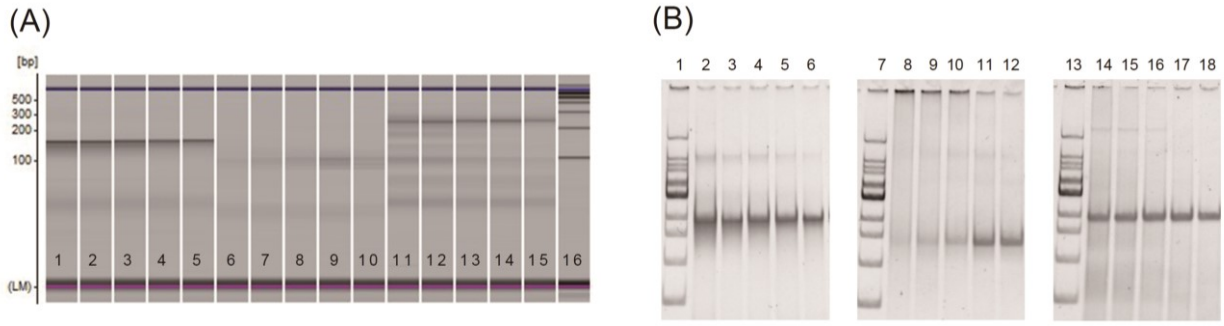

Figure 2. Electrophoretic analysis of tetrapodna, tetrahedron, and tetragon. (A) Aliquots of tetrapodna, tetrahedron, and tetragon (68 ng) prepared at 0.5–20 μM DNA were run on a MultiNA microchip electrophoresis system. Lanes 1–5, tetrapodna (20, 10, 5, 1, and 0.5 μM); lanes 6–10, tetrahedron (20, 10, 5, 1, and 0.5 μM); lanes 11–15, tetragon (20, 10, 5, 1, and 0.5 μM); lane 16, 100-bp DNA ladder. (B) Aliquots of tetrapodna, tetrahedron, and tetragon (68 ng) prepared at 0.5–20 μM DNA were run on a PAGE. Lanes 1, 7, and 13, 100-bp ladder, lanes 2–6, tetrapodna (20, 10, 5, 1, and 0.5 μM); lanes 8–12, tetrahedron (20, 10, 5, 1, and 0.5 μM); lanes 14–18, tetragon (20, 10, 5, 1, and 0.5 μM).

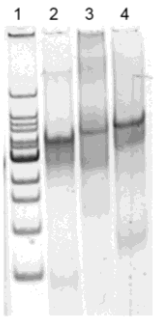

Figure 3. Electrophoretic analysis of tetrapodna, tetrahedron, and tetragon for AFM. Aliquots of tetrapodna, tetrahedron, and tetragon for AFM prepared at 1 μM DNA were run on a PAGE. Lane 1, 100-bp ladder; lane 2, tetrapodna; lane 3, tetrahedron; lane 4, tetragon.

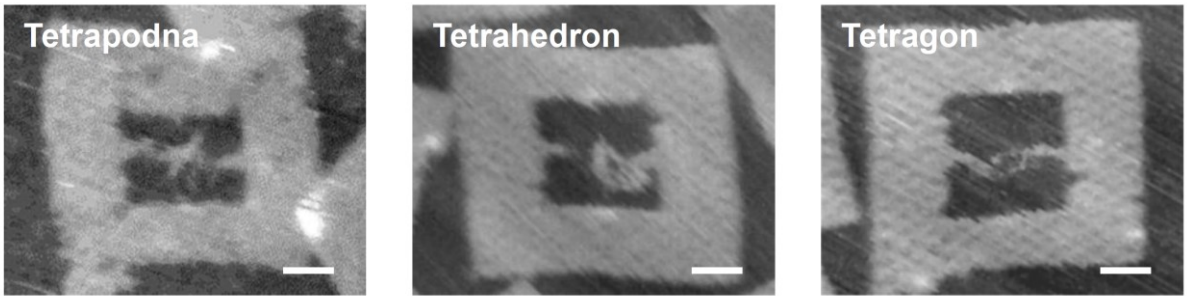

Figure 4. AFM images of tetrapodna, tetrahedron, and tetragon. The white rectangles with a window represent DNA origami frames. All DNA samples were annealed at a DNA concentration of 1 μM to exclude the higher structures/aggregates of tetrahedron. The white bars indicate 20 nm.

The mobility was the fastest for tetrahedron, followed by tetrapodna, then tetragon. These differences would be due to the structural differences of these DNA nanostructures, as all these DNA nanostructures consisted of 220 nucleotides. Figure 2B shows the PAGE analysis of these DNA nanostructures prepared at DNA concentration of 0.5–20 μM. A significant fraction of tetrahedron remained in the well, suggesting that it formed multimers or aggregates under these conditions at high DNA concentrations. The formation of tetrapodna, tetrahedron, and tetragon was confirmed using AFM. The PAGE analysis of DNA nanostructures for AFM experiments was shown in Figure 3. A DNA frame prepared using the DNA origami method was used to immobilize the DNA nanostructures for imaging. In addition, two of the four ODNs for each DNA nanostructure were extended to be immobilized to the frame. Figure 4 shows the AFM images of tetrapodna, tetrahedron, and tetragon immobilized to the DNA frame. AFM images with large area were shown in Figure 5.

Figure 5. AFM images of tetrapodna, tetrahedron, and tetragon. The white rectangles with a window represent DNA origami frames.

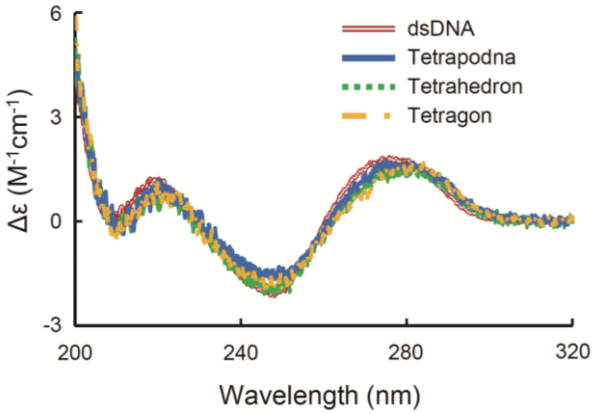

Figure 6. CD spectra of tetrapodna, tetrahedron, and tetragon. CD spectra were recorded using a JASCO-820 type spectropolarimeter. To facilitate comparisons, the background of CD spectra was subtracted.

The images clearly show that all of the preparations had different structures from one another. Tetrapodna was structured with four pods extruding from the center, the structural characteristics of which were almost identical to those of a larger tetrapodna consisting of 90-base ODNs[24]. The AFM image of tetragon shows a rectangular shape as designed. On the other hand, the image for tetrahedron shows a triangular structure that was more complicated than the others.

I-1-3-b. Tm and apparent size of DNA nanostructures

The thermal stabilities of tetrapodna, tetrahedron, and tetragon were examined by measuring the Tm. Table 2 summarizes the Tm values in TE buffer containing 50 mM magnesium chloride. Tetrapodna had the highest Tm, followed by tetragon. The apparent sizes of these DNA nanostructures, measured by dynamic light scattering, are also listed in Table 2. All preparations were about 8 nm in diameter.

Table 2. Tm and apparent size of tetrapodna, tetrahedron, and tetragon.

DNA	Tm (°C)	Size (nm)
Tetrapodna	**77.4**	**7.4 ± 0.8**
Tetrahedron	**68.3**	**8.5 ± 0.9**
Tetragon	**73.0**	**8.4 ± 1.0**

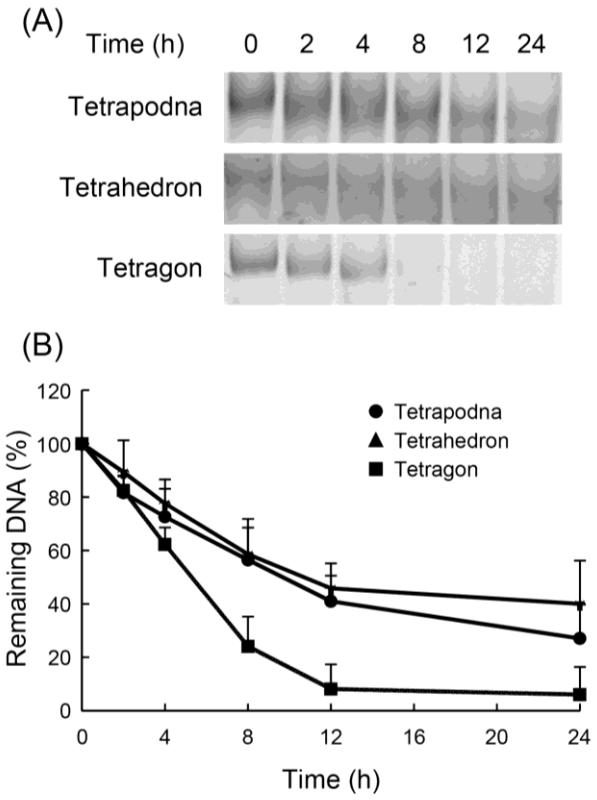

Figure 7. Degradation of tetrapodna, tetrahedron, and tetragon in 50% non-heat-inactivated FBS. (A) Each sample incubated at 37°C for indicated times was run on 9% polyacrylamide gel and stained with SYBR Gold. PAGE results are representative of five independent experiments. (B) The density of full-length DNA bands was quantitatively evaluated using the Multi Gauge software. The remaining amounts of full-length DNA were plotted against the incubation time. Results are expressed as mean + SEM of five independent experiments.

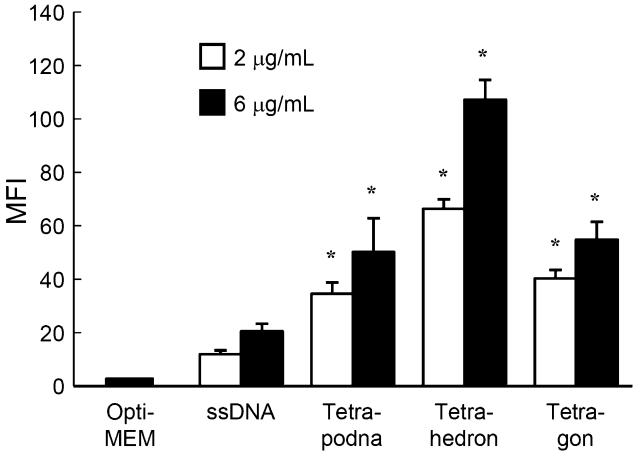

Figure 8. Uptake of ssDNA (ODN-1-1-1), tetrapodna, tetrahedron, and tetragon in RAW264.7 cells. Each Alexa Fluor 488-labeld DNA sample was added to cells at a final concentration of 2 or 6 μg/mL. Non-labeled ODNs were added to Alexa Fluor 488-labeld ssDNA to adjust the amount of the fluorescently labeled DNA added to the cells. The MFI of RAW264.7 cells was measured as an index of cellular uptake (n = 4 per group). Results are expressed as mean + SEM of three independent experiments. *P < 0.05 compared with ssDNA at the same concentration.

I-1-3-c. CD spectra of DNA nanostructures

Figure 6 shows the CD spectra of tetrapodna, tetrahedron, and tetragon. All samples examined had a positive peak near 280 nm and a negative peak near 240 nm, and there were no significant differences in the spectra. The spectra of the DNA nanostructures were similar to those of dsDNA, which exhibited B-form under the conditions examined.

I-1-3-d. Stability of DNA nanostructures in serum

Figure 7A shows the PAGE analysis of the DNA nanostructures incubated in solution containing 50% non-heat-inactivated FBS. The bands of the DNA nanostructures weakened with time in all cases. In addition, the bands shifted down with time because of the degradation of the DNA nanostructures. Figure 7B shows the time-courses of the remaining DNA after densitometric analysis of the gels. This analysis indicated that tetragon was quickly degraded with time compared with the others.

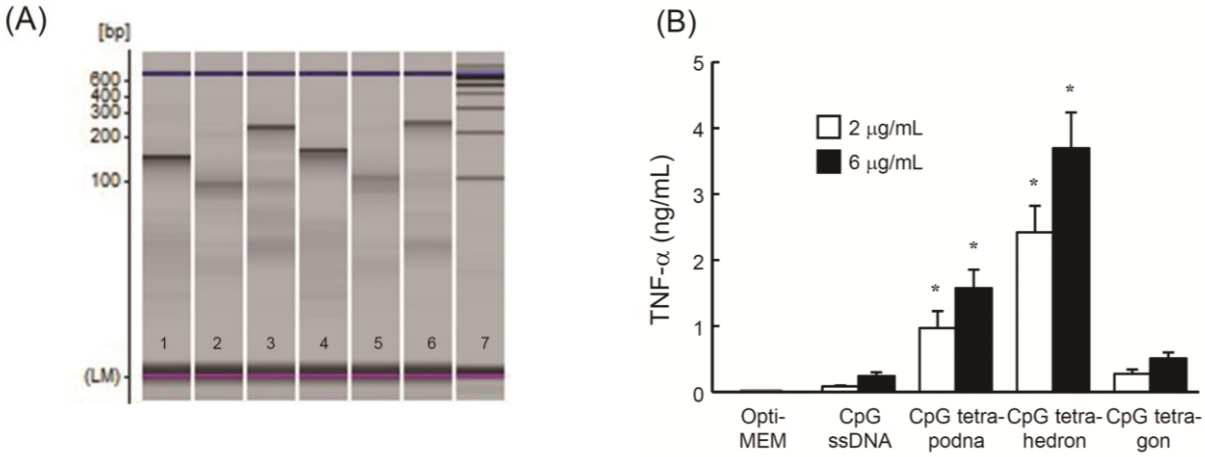

Figure 9. Preparation of CpG tetrapodna, CpG tetrahedron, and CpG tetragon and TNF-α release after addition of CpG DNAs to RAW264.7 cells. (A) Aliquots of tetrapodna, tetrahedron, and tetragon with (75 ng) or without CpG DNA (68 ng) prepared at 1 μM DNA were run on a MultiNA microchip electrophoresis system. Lane 1, tetrapodna; lane 2, tetrahedron; lane 3, tetragon; lane 4, CpG tetrapodna; lane 5, CpG tetrahedron; lane6, CpG tetragon; lane 7, 100-bp DNA ladder. (B) Each DNA sample was added to cells at a final concentration of 2 or 6 μg/mL, and the concentrations of TNF-α in the supernatant were measured at 8 h (n = 4 per group). Non-CpG ODNs were added to CpG ssDNA to adjust the amount of the CpG DNA added to the cells. Results are expressed as mean + SEM of four independent experiments. *P < 0.05 compared with ssDNA at same concentration.

I-1-3-e. Uptake of Alexa Fluor 488-labeled DNA nanostructures in RAW264.7 cells

Figure 8 shows the MFI of RAW264.7 cells after addition of Alexa Fluor 488-labeled DNA samples. RAW264.7 cells with added Alexa Fluor 488-labeled tetrahedron showed the highest MFI value, followed by Alexa Fluor 488-labeled tetrapodna, tetragon, and ssDNA (ODN-1-1-1) in this order. The MFI values increased with increasing DNA concentration from 2 to 6 μg/mL in all the cases.

I-1-3-f. TNF-α release from RAW264.7 cells after addition of CpG DNA nanostructures

Figure 9A shows the MultiNA analysis of tetrapodna, tetrahedron, and tetragon with an extending 25-base long sequence containing a CpG motif (Figure 10 shows the PAGE analysis of these DNA nanostructures). Each DNA nanostructure containing CpG DNA was named as CpG tetrapodna, CpG tetrahedron, and CpG tetragon, respectively. Figure 9B shows the amount of TNF-α released from RAW264.7 cells after addition of CpG ssDNA (CpG ODN-1-1-1), CpG tetrapodna, CpG tetrahedron, or CpG tetragon. Compared with CpG ssDNA, all of the CpG DNA nanostructures induced high amounts of TNF-α. CpG tetrahedron induced the largest amounts of TNF-α, followed by CpG tetrapodna. CpG tetragon induced much less TNF-α release from RAW264.7 cells than CpG tetrapodna did, even though there were no significant differences in the uptake between Alexa Fluor 488-labaled tetrapodna and tetragon (Figure 8). Tetrapodna, tetrahedron, or tetragon containing no CpG motifs induced little TNF-α release when added to RAW264.7 cells (data not shown).

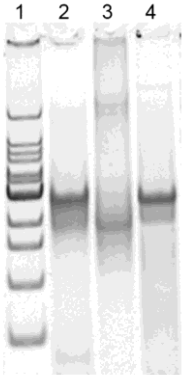

Figure 10. Electrophoretic analysis of CpG tetrapodna, CpG tetrahedron, and CpG tetragon. Aliquots of CpG tetrapodna, CpG tetrahedron, and CpG tetragon (68 ng) prepared at 1 μM DNA were run on a PAGE. Lane 1, 100-bp ladder; lane 2, CpG tetrapodna; lane 3, CpG tetrahedron; lane 4, CpG tetragon.

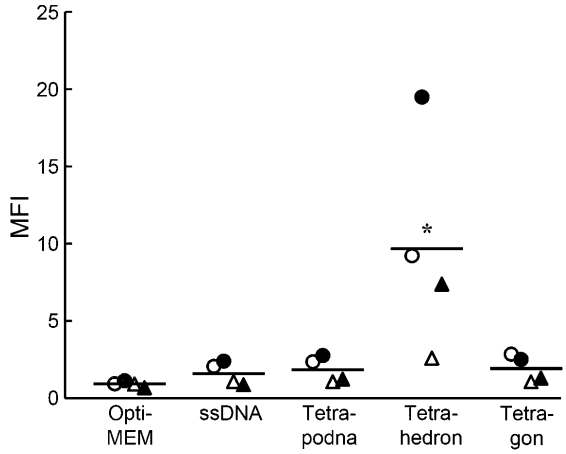

Figure 11. Uptake of ssDNA (ODN-1-1-1), tetrapodna, tetrahedron, and tetragon in human PBMCs. Each Alexa Fluor 488-labeld DNA sample was added to cells at a final concentration of 6 μg/mL. Non-labeled ODNs were added to Alexa Fluor 488-labeld ssDNA to adjust the amount of the fluorescently labeled DNA added to the cells. The MFI of PBMCs was measured as an index of cellular uptake (n = 4 per group). Each symbol represents a mean of a single experiment, and each experiment is identified with different symbols. Bars represent the mean of four independent experiments. *P < 0.05 compared with ssDNA.

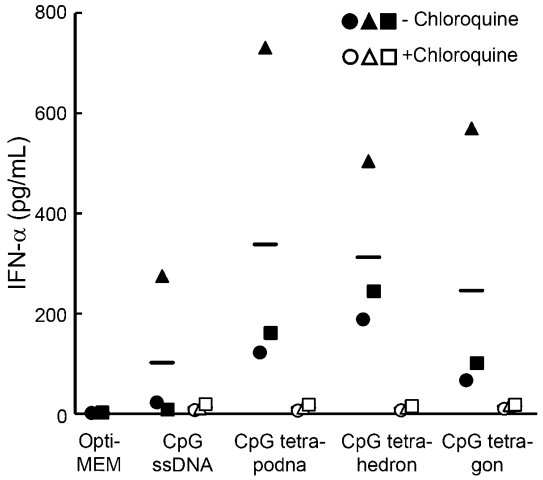

Figure 12. IFN-α release after addition of CpG DNAs to human PBMCs with or without treatment with 100 μM chloroquine. Each DNA sample was added to cells at a final concentration of 6 μg/mL, and the concentrations of IFN-α in the supernatant were measured at 24 h (n = 4 per group). Non-CpG ODNs were added to CpG ssDNA to adjust the amount of the CpG DNA added to the cells. Each symbol represents a mean of a single experiment, and each experiment is identified with different symbols. Bars represent the mean of three independent experiments.

I-1-3-g. DNA uptake and IFN-α release after addition of DNA nanostructures to human PBMCs

Figure 11 shows the MFI of human PBMCs after addition of Alexa Fluor 488-labeled DNA samples. PBMCs with added Alexa Fluor 488-labeled tetrahedron showed the highest MFI value. The MFI values of PBMCs added with either Alexa Fluor 488-labeled ssDNA (ODN-1-1-1), tetrapodna, or tetragon were comparable to one another. Figure 12 shows the amount of IFN-α released from RAW264.7 cells after addition of CpG ssDNA (CpG ODN-1-1-1), CpG tetrapodna, CpG tetrahedron, or CpG tetragon in the absence or absence of chloroquine. All of the CpG DNA nanostructures induced high amounts of IFN-α compared with CpG ssDNA (CpG ODN-1-1-1). IFN-α release was greatly inhibited by chloroquine.

I-1-4 Discussion

The versatility of DNA nanotechnology makes it possible to design DNA nanostructures of any shape because the number of ODNs as well as their sequence and length can be arbitrarily selected. This is one of the major advantages of DNA nanotechnology, and it was used in the present study to construct and compare three different DNA nanostructures. However, a set of ODNs used for a DNA nanostructure cannot be used to construct other nanostructures, and a different set of ODNs should be prepared for each DNA nanostructure. This difference should be kept in mind when the structural properties of DNA nanostructures are compared with one another. In this study, one of the four ODNs was used for all the three DNA nanostructures to minimize the differences in the sequence of the ODNs. In addition, the GC content, which is a key parameter determining the thermal stability of

the structures, was adjusted to be comparable among the three DNA nanostructures between 45% and 47%. Finally, the lack of significant TNF-α release from cells added with any DNA nanostructure containing no CpG motifs indicated that TNF-α release after addition of the CpG DNA nanostructures could be attributed to the CpG motif.

A set of ODNs reported by Li et al. was selected for the comparison because our preliminary studies showed that tetrahedron had much lower flexibility in design than tetrapodna. For example, tetrahedron was not obtained when four 43-mer ODNs were used (Ohtsuki et al., unpublished results), whereas tetrapodna could be formed using four ODNs from 36 to 90-mer ODNs[24]. In addition, the present study revealed that high ODN concentrations resulted in the formation of multimers or aggregates except for tetrapodna, greatly limiting the conditions for preparing the DNA nanostructures for comparison, even though preparation efficiency is one of the most important parameters as far as biopharmaceutical applications are concerned.

Structures other than those examined in this study can also be designed using four 55-mer ODNs. A simpler structure is a linear one partly or fully containing double-stranded DNA. The structural properties of such linear DNA would be similar to those of double-stranded DNA, and therefore, it was not included for comparison in this study. Other structures would share the structural properties with either tetrapodna (branched DNA), tetrahedron (three-dimensional DNA), or tetragon (rectangular or circular DNA), as far as symmetric structures are concerned. Therefore, the three DNA nanostructures would be reasonable for comparing the structural and biological properties of DNA nanostructures that were designable using four short ODNs.

The present study clearly demonstrated that tetrapodna was far the best DNA nanostructure in terms of both the preparation efficiency and biological activity. This would be, at least in part, attributed to its high thermal stability (Table 2). The lengths of the consecutive double-stranded parts in each structure were 27, 17, and 26 for tetrapodna, tetrahedron, and tetragon, respectively, and the long double-stranded parts could explain the high Tm value of tetrapodna. The Tm values of the incomplete structures consisting of three out of four ODNs were 73°C, 68°C, and 71°C for tetrapodna, tetrahedron, and tetragon, respectively. In addition, the Tm values of the 27-mer double-stranded DNA identical to a branch of tetrapodna and 26-mer double-stranded DNA identical to a side of tetragon were 72°C and 70°C, respectively. These results strongly indicated that the complete structure of tetrapodna was more thermally stable than the incomplete ones. This unique property is a reason for the very high preparation efficiency of tetrapodna, even at high DNA concentrations. In contrast, the others were not stabilized by the formation of complete structures, which led to the formation of multimers/aggregates at high DNA concentrations.

The above discussions on the thermal stability suggested that it is difficult to re-design tetrahedron with high preparation efficiency even at high DNA concentrations. Li et al. reported that tetrahedron could be obtained by self-assembly of four ODNs, but the authors prepared tetrahedron at a low DNA concentration of 1 μM[32]. As demonstrated in the present study, increasing the DNA concentration reduced the preparation efficiency

of tetrahedron. Any approach to avoid the oligomerization of tetrahedron would greatly expand its usefulness as delivery vehicles to immune cells.

DNA nanostructures, including tetrahedron, were considered to be monomer under the experimental conditions examined, but the possibility that they form multimers or aggregates at their interaction with cells cannot be excluded at this moment. Therefore, there is still a possibility that the efficient cellular uptake of tetrahedron is due to its more efficient formation of multimers or aggregates than the others.

Previous study from my laboratory on the interaction of polypodnas with immune cells, including RAW264.7 cells and mouse bone marrow-derived dendritic cells, indicated that DNA assemblies with bulky structures were more efficiently taken up by the cells compared with ones with sparse structures[22–25]. A previous study reported that longer DNA was better than short ones in terms of cellular uptake[24]. Several receptors or membrane proteins have been reported to be involved in the cellular uptake of DNA[35,36], although no consensus applicable to various cells has been reached yet. However, the results of the cellular uptake of DNA preparations suggested that the interaction of DNA with the cell surface at multiple sites facilitated its cellular uptake. The present study showed that tetrahedron was better than tetrapodna in terms of the uptake by RAW264.7 cells (Figure 8). The formation of oligomers might be involved in the efficient uptake of tetrahedron, even though tetrahedron was prepared under conditions where multimers were not easily formed (Figure 2A, lane 9). The reason for this efficient cellular uptake of tetrahedron requires further investigation.

The experimental results obtained with human PBMCs showed large variations compared to those with RAW264.7 cells, probably because of intraindividual and/or interindividual variability in the property of the cells. Generally speaking, however, the results were comparable to those with RAW264.7 cells, suggesting that the DNA nanostructures examined in this study, especially CpG tetrapodna and CpG tetrahedron, induce cytokines, including IFN-α, in humans more efficiently than CpG ssDNA. The substantial inhibition of IFN-α release from human PBMCs by chloroquine, an inhibitor of endosomal TLR signaling, strongly suggests that the TLR9 is involved in the IFN-α release from the cells after addition of CpG tetrapodna, CpG tetrahedron or CpG tetragon. In contrast, the uptake of Alexa Fluor488-labeled tetrapodna and tetragon by human PBMCs was comparable to that of Alexa Fluor488-labeled ssDNA, which was different from the results obtained using RAW264.7 cells (Figure 11), A possible explanation on this difference is that the population of cells that can be responsible for stimulation with CpG DNA in PBMCs, i.e., plasmacytoid dendritic cells, is quite low[37]. Higher uptake of Alexa Fluor488-labeled tetrahedron than the others may indicate that tetrahedron is efficiently taken up not only by plasmacytoid dendritic cells but by other cells in PBMCs.

The present study clearly showed that tetrapodna had the highest thermal stability, best formation efficiency, and CpG tetrapodna possessed high potency to induce TNF-α release from RAW264.7 cells and IFN-α release from PBMCs. Despite efficient cellular uptake and TNF-α release, the low formation efficiency of tetrahedron greatly limited its application as a delivery vehicle of immunostimulatory DNAs. CpG tetragon was the least efficient in terms of TNF-α release. Taken together, I conclude that tetrapodna is the best assembly as

delivery vehicles for immunostimulatory nucleic acids to immune cells, and that tetrahedron can be another useful assembly for cellular delivery if its preparation yield is improved[38].

Chapter I

Section 2

Effect of the structural properties of tripod-like structured DNA on their interaction with macrophage-like RAW264.7 cells

I-2-1 Introduction

In Section 1, correlation was obtained between the structural properties and cellular uptake of nanostructured DNA. However, it is not clear which structural features of the three-dimensional structure are important, and elucidation is required. The aim of this section was to describe what kind of properties increase the uptake of nanostructured DNA and cytokine release. To solve this question, I selected tripod-like structured DNA (tripodna) as a three-dimensional nanostructured DNA that can be easily evaluated and evaluated the effect of the structural featured of tripodna on the interaction of tripodna and the cells. In this section, I designed several types of tripodna and DNA assemblies consisting of double-stranded DNA or nick double-stranded DNA.

I-2-2 Materials and Methods

Chemicals

All chemicals were the highest grade available and used without further purification as described in Chapter I, Section 1.

Cell culture

The murine macrophage-like cell line RAW264.7 was cultured as described in Chapter I, Section 1. RAW264.7 cells were then plated on 24-well or 96-well culture plates at a density of 5×10^5 cells/mL and cultured for 24 h prior to use.

Oligodeoxynucleotides

All ODNs used were purchased from Integrated DNA Technologies, Inc.. The sequences of the ODNs used are listed in Table 3. For cellular uptake experiments, ODN-1-2-1 labeled with Alexa Fluor-488 at the 5′ end (Alexa ODN-1-2-1) was purchased from Japan BioService Co., Ltd..

Preparation of DNA nanostructures

ODNs dissolved in an annealing buffer (TE buffer; 10 mM Tris-HCl, pH 8, 1 mM ethylenediaminetetraacetic acid (EDTA), and 50 mM magnesium chloride) were mixed at a final concentration of 100 μM for each ODN. The annealing buffer was used to prepare all the DNA samples. The mixtures were then

incubated at 95°C for 2 min and slowly cooled down to 4°C using a thermal cycler. Each preparation was analyzed by 6% polyacrylamide gel electrophoresis.

Measurement of melting temperature

The melting temperatures (Tm) were obtained by measuring the absorbance of nanostructured DNAs in TE buffer as described in Chapter I, Section 1.

Cellular uptake of DNA

RAW264.7 cells on 96-well plates at a density of 5×10^4 cells/well were incubated with Alexa Fluor 488-labeled single-stranded DNA (ssDNA) or tripodnas diluted in 0.1 mL of Opti-MEM for 2 h at 37°C. Cells were then washed three times with 200 μL of phosphate-buffered saline and harvested. Then, the fluorescent intensity of cells was determined by flow cytometry (Gallios Flow Cytometer) using Kaluza software, and the mean fluorescence intensity (MFI) was calculated.

TNF-α release from RAW264.7 cells

RAW264.7 cells were seeded into 96-well plates at a density of 5×10^4 cells/well. Then, ssDNA or tripodnas was diluted in 0.1 mL of Opti-MEM and added to the cells. The cells were incubated at 37°C for 8 h, and the supernatants were retrieved and stored at -80°C until use. The levels of TNF-α in the supernatants were determined by enzyme-linked immunosorbent assay (ELISA) as described in Chapter I, Section 1.

Statistical analysis

Differences were statistically evaluated by one-way analysis of variance (ANOVA) followed by the Tukey-Kramer test for multiple comparisons. A P value of <0.05 was considered statistically significant.

Table 3. The sequences of ODNs for DNA nanostructures.

Name	Sequences (5′ → 3′)	Length (mer)
ODN-1-2-1 (a)	GCTAGACGTTCCATACCTTCCTAAGGTAGCAGCTAG	36
ODN-1-2-2 (b)	CTAGCTGCTACCTTAGGAAGGTATGGAACGTCTAGC	36
ODN-1-2-3 (c)	AGGTATGGAACGTCTAGC	18
ODN-1-2-4 (d)	CTAGCTGCTACCTTAGGA	18
ODN-1-2-5 (e)	GTGAGTAGAGGTATGGAACGTCTAGC	26
ODN-1-2-6 (f)	CTAGCTGCTACCTTAGGACTACTCAC	26
ODN-1-2-7 (g)	TAGGGTGAGTAGAGGTATGGAACGTCTAGC	30
ODN-1-2-8 (h)	CTAGCTGCTACCTTAGGACTACTCACCCTA	30
ODN-1-2-9 (i)	AGGTTCTAGGGTGAGTAGAGGTATGGAACGTCTAGC	36
ODN-1-2-10 (j)	CTAGCTGCTACCTTAGGACTACTCACCCTAGAACCT	36

All ODNs have a phosphodiester backbone. Underlined is the CpG motif (GACGTT). ss36=a, ds36=a+b, ds36/18,18=a+c+d, tripodna36/26/26=a+e+f, tripodna36/30/30=a+g+h, tripodna36=a+i+j.

I-2-3 Results

I-2-3-a. Structural characteristics of partial tripodna

Figure 13 indicates schematic images of DNA assemblies. The sequences of the ODNs are listed in Table3. In Figure 14, formation of all DNA assemblies were confirmed by PAGE. The band showed that complementary tripodna had more bulky structure than tripodna with partial structures.

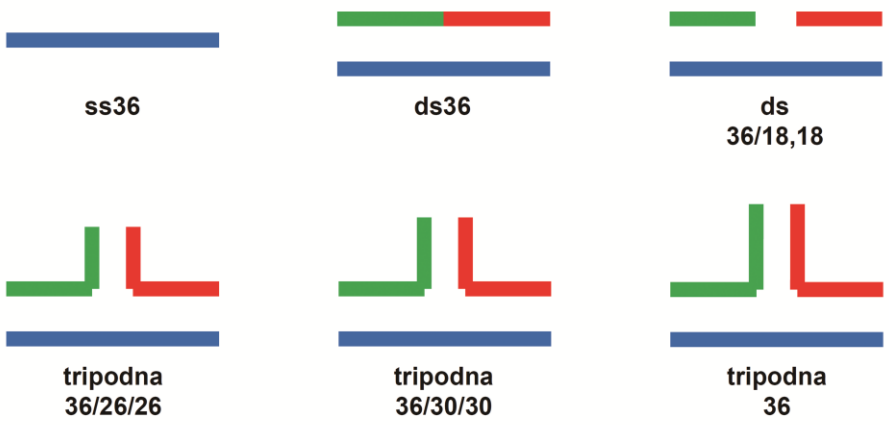

Figure 13. Schematic presentation of nanostructured DNA. The blue-colored ODNs are the common ODN.

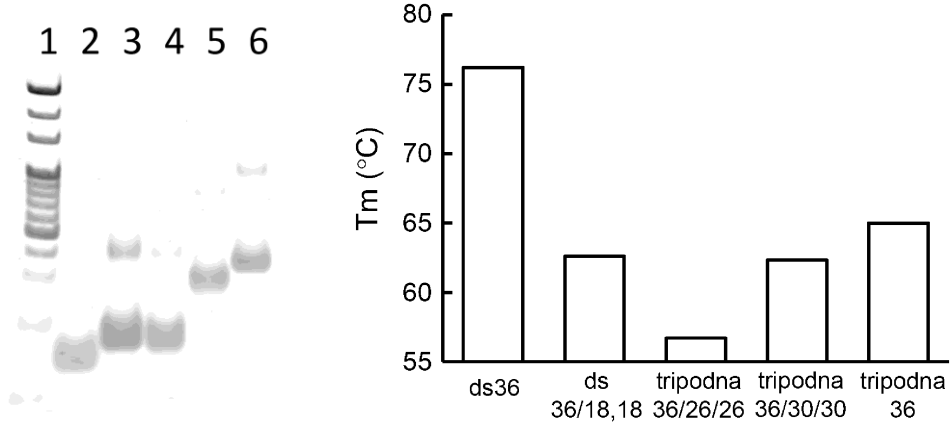

Figure 14. PAGE analysis of nanostructured DNAs. Lane 1, 20-bp ladder; lane 2, ds36; lane 3, ds36/18,18; lane4, tripodna36/26/26; lane 5, tripodna36/30/30; lane6, tripodna36.

Figure 15. Melting temperature (Tm) of nanostructured DNAs.

I-2-3-b. Tm of DNA assemblies

The thermal stabilities of DNA assemblies were evaluated by measuring the Tm. Figure 15 summarizes the Tm values in TE buffer containing 50 mM magnesium chloride. Double-stranded DNA (dsDNA) had the highest Tm, because dsDNA had longest double strand. The presence of partial structure reduced thermal stability. These results indicate that the hybridization of every ODN consisting of a tripodna greatly increases the structural stability of tripodna preparations.

I-2-3-c. Uptake of Alexa Fluor 488-labeled tripodna and uncomplimentary tripodna

Figure 16 shows the MFI of RAW264.7 cells after addition of Alexa Fluor 488-labeled DNA assemblies. RAW264.7 cells with added nanostructured DNAs with bended pods showed higher MFI value than dsDNA or

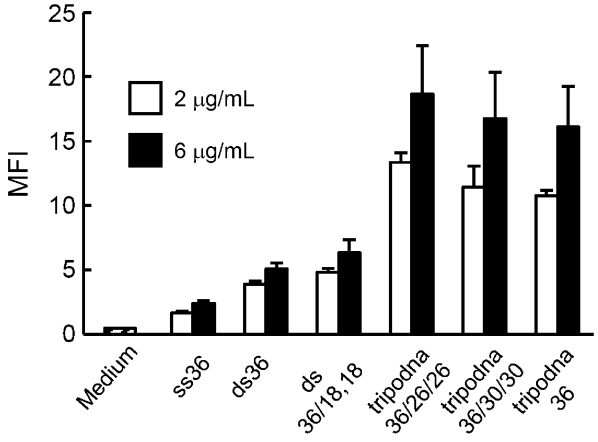

Figure 16. Uptake of ss36, ds36, ds36/18,18, tripodna36/26/26, tripodna36/30/30, and tripodna36. Each Alexa Fluor 488-labeld DNA sample was added to cells at a final concentration of 2 or 6 μg/mL. Results are expressed as mean + S.D. (n=4)

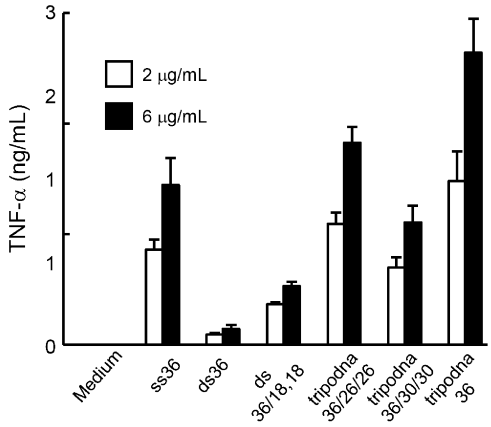

Figure 17. Each DNA sample was added to cells at a final concentration of 2 or 6 μg/mL, and the concentrations of TNF-α in the supernatant were measured at 8 h (n = 4 per group). Results are expressed as mean + S.D.

ssDNA. The MFI values increased with increasing DNA concentration from 2 to 6 μg/mL in all the cases.

I-2-3-d. TNF-α release from RAW264.7 cells

Figure 17 shows the amount of TNF-α released from RAW264.7 cells after addition of nanostructured DNA. Compared with complementary tripodna, the presence of partial structure reduces the cytokine release of CpG DNA.

I-2-4 Discussion

In this section, I aimed to elucidate the structural property of nanostructured DNA. To simplify the evaluation, I picked up tripod-like structured DNA.

A previous study from my laboratory reported that hexapod-like structured DNA showed efficient interaction with immune cells compared with tripod-like structured DNA, or tetrapod-like structured DNA preparations of same length of ODNs[24]. The effect of size on cellular uptake has been described so far[39–41], but detailed information about the recognition of 3D-structure of polypod-like structured DNA was missing. In Section 1, I revealed that the structural property of nanostructured DNA could affect the interaction with immune cells. In this section, I selected tripod-like structured DNA to examine the details on the structural properties of nanostructured DNA required for the cellular uptake.

A previous study reported that DNA with a neck had a low melting temperature (Tm) compared with double stranded DNA with no neck strcutures[42]. Experiments using asymmetric tripodna preparations showed that the Tm was a function of the length of the neck and using a length half that of the other parts resulted in a minimal Tm value (Figure 15). The presence of a short neck would force the double stranded DNA to bend, but it would not help the structure to be stabilized because the length is too short. Taken together, the Tm of polypodna is a complicated function of the bend angle and the length of each pod.

TLR9 recognition of CpG DNA occurs after endocytosis and the dissociation of double-stranded DNA into single strands depends on the endosomal environments. In this study, double-stranded DNA with a nick made with three ODNs was also used in addition to completely complementary double-stranded DNA, because the former seems to be more easily dissociated into single strands than the latter.

In both studies of cellular uptake and cytokine release, tripodna with a perfect structure had the highest values in terms of cell interaction and subsequent cytokine production.

In this section, I concluded that bent DNA structures are efficiently recognized by RAW264.7 cells than linear ones.

Chapter I

Section 3

Elucidation of the mechanism of increased activity of immunostimulatory DNA by the formation of polypod-like structure.

I-3-1 Introduction

In Section 1 and 2, the results suggested that nanostructured DNA including polypod-like structured DNA is useful for delivery of nucleic acid drugs to macrophage-like RAW264.7 cells. However, for clinical use, it is also necessary to evaluate by cells other than target cells. Moreover, the uptake pathways of nanostructured DNA need to be clarified. To elucidate the mechanism of increased immunostimulatory DNA activity by the formation of polypod-like structures, I selected two types of polypodna: tripodna and hexapodna. I examined their uptake in several types of immune and non-immune cells. Then, I also tested other type of nanostructured DNA including tetrapodna, tetrahedron, and tetragon same as Section 1 to elucidate the influence of structural properties on cellular uptake.

I-3-2 Materials and Methods

Chemicals

RPMI1640 medium and Dulbecco's modified Eagle's medium (DMEM) were obtained from Nissui Pharmaceutical Co., Ltd.. Fetal bovine serum (FBS) was obtained from Equitech-Bio Inc. (Kerrville, TX, USA). Dextran sulfate sodium salt (109-12, average molecular weight of 150 kDa) was purchased from Nacalai Tesque (Kyoto, Japan). All other chemicals were of the highest grade available and used without further purification as described in Chapter I, Section 1.

Cell culture

Mouse aorta endothelial MAEC cells were kindly provided by Professor Ichiro Saito (School of Dental Medicine, Tsurumi University, Yokohama, Japan) and maintained in Medium 199 (M199: Life Technologies, Tokyo, Japan) containing 10% heat-inactivated FBS, 0.2% $NaHCO_3$, 100 U/mL penicillin, and 100 mg/mL streptomycin. Mouse yolk sac endothelial C166 cells were cultured in DMEM supplemented with 10% heat-inactivated FBS, 0.15% $NaHCO_3$, 100 units/mL penicillin, 100 mg/mL streptomycin, 4 mM L-glutamine, 4500 mg/L glucose, and 1 mM sodium pyruvate. Mouse macrophage-like RAW264.7 cells were cultured as described in Chapter I, Section 1. Mouse dendritic DC2.4 cells were kindly provided by Dr. K. L. Rock (University of Massachusetts Medical School, Worcester, MA, USA). DC2.4 cells were cultured in RPMI1640 supplemented with 10% heat-inactivated FBS, 50 μM monothioglycerol, antibiotics, L-glutamine, and

non-essential amino acids (Gibco, Eggenstein, Germany). Mouse embryonic fibroblast NIH3T3 cells and C2C12 cells were cultured in DMEM containing 4.5 g/L glucose and L-glutamine supplemented with 10% heat-inactivated FBS, 0.3% $NaHCO_3$, 100 units/mL penicillin, and 100 mg/mL streptomycin. HEK-Blue hTLR9 cells were obtained from InvivoGen. The cells were cultured in DMEM supplemented with 10% heat-inactivated FBS, 0.2% sodium bicarbonate, 100 IU/mL penicillin, 100 μg/mL streptomycin, 2 mM L-glutamine, 10 mg/mL blasticidin, 100 mg/mL zeocin, and 50 mg/mL normocin. All cells were cultured at 37°C in a humidified atmosphere of 5% CO_2, and then cells were seeded on 48-well or 96-well culture plates at a density of 5×10^5 cells/mL and cultured for 24 h prior to use.

Oligodeoxynucleotides

Phosphodiester oligodeoxynucleotides (ODNs) were purchased from Integrated DNA Technologies, Inc.. In this study, the following DNA samples were prepared: ssDNA, dsDNA, tripodna, and hexapodna. For cellular uptake experiments, same ODNs as Section 1 were prepared: ssDNA, tetrapodna, tetrahedron, and tetragon.

Preparation of polypodna

Polypodna was prepared by mixing equimolar amounts of corresponding ODNs as previously described. In brief, ODNs were dissolved in TE buffer (10 mM Tris-HCl, 1 mM ethylenediaminetetraacetic acid (EDTA), pH 8) to obtain stock solutions of each ODN at a concentration of 0.1 mM. Then, ODNs were mixed and the salt concentration was adjusted to 5 or 150 mM (sodium chloride) or 15 mM (magnesium chloride). Mixtures were then incubated at 95°C for 5 min, then slowly cooled to 4°C using a thermal cycler.

Cellular uptake of DNA

Cells were seeded at a density of 5×10^4 cells/well in 96-well plates and incubated for 24 h at 37°C. The culture medium was replaced with Opti-MEM containing Alexa Fluor 488-labeled polypodna, tetrahedron, or tetragon and the cells were incubated for 2 h at 37°C. Cells were then washed twice with 200 μL phosphate-buffered saline (PBS) and harvested. Then, the fluorescence intensity of cells was determined by flow cytometry (FACS Calibur or Gallios Flow Cytometer) using CellQuest software (version 3.1, BD Biosciences) or Kaluza software, and the mean fluorescence intensity (MFI) was calculated.

Effect of dextran sulfate on the cellular uptake of DNA in RAW264.7 cells

RAW264.7 cells were seeded at a density of 1×10^5 cells/well in 48-well plates and incubated for 24 h at 37°C. Dextran sulfate (DS) was used as an inhibitor of type A scavenger receptor (SR-A) to examine the involvement of SR-A in the cellular uptake of polypodna preparations[43]. Cells were preincubated for 30 min with 5 mg/mL DS, then washed twice with 200 μL PBS, and the cellular uptake of DNA was examined as described above.

Confocal microscopic observation of nanostructured DNAs

RAW264.7 cells or NIH3T3 cells were seeded on a chamber slide at a density of 3×10^4 cells/well and then cultured for 24 h. The concentration of Alexa Fluor 488-labeled tetrapodna, tetrahedron, or tetragon was adjusted to 2 μg/mL in Opti-MEM. The medium on the slides was removed, and samples were applied to RAW264.7 cells, and then incubated at 37 °C for 2 h. The cells were washed twice with phosphate-buffered saline (PBS), fixed with 4% paraformaldehyde for 20 min, and washed again twice with PBS. The cells were then blocked with 20% FBS in PBS for 1 h. The cells were incubated with 600 nM 4′,6-diamidino-2-phenylindole (DAPI; Life Technologies) for 5 min at room temperature and washed once. The chamber was then removed and the slide was observed using a confocal microscope (A1R MP, Nikon Instech Co., Ltd., Tokyo, Japan) as previously reported[44].

Examination of the uptake pathway of nanostructured DNA

RAW264.7 cells or NIH3T3 cells were seeded at a density of 1×10^5 cells/well in 48-well plates and incubated for 24 h at 37°C. Cells were pretreated with 100 μM mono dansyl cadaverine (clathrin-mediated endocytosis inhibitor), 100 μg/mL nystatin (caveolae-mediated endocytosis inhibitor), or 15 μg/mL cytochalasin B (actin depolymerization inhibitor) for 30 min. Then, the culture medium was replaced with Opti-MEM containing Alexa Fluor 488-labeled polypodna, tetrahedron, or tetragon with uptake inhibitor, and the cells were incubated for 2 h at 37°C.

Statistical analysis

Differences were statistically evaluated by one-way analysis of variance (ANOVA) followed by the Tukey–Kramer tests for multiple comparisons. $P < 0.05$ was considered to be statistically significant.

I-3-3 Results

I-3-3-a. Cellular uptake of DNA samples with diverse structural properties in various cell lines

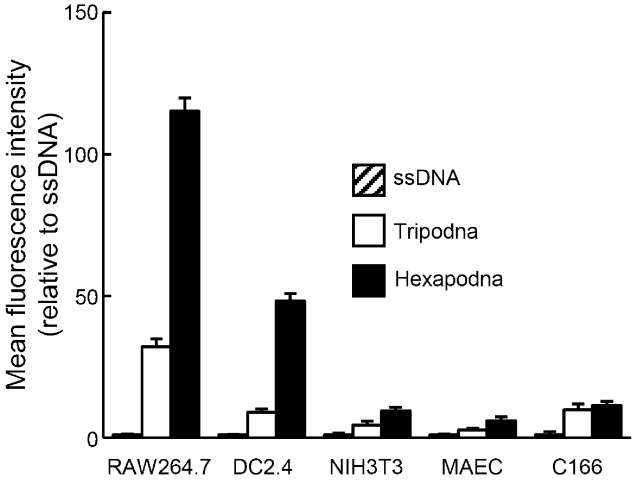

Figure 18. Uptake of nanostructured DNAs in immune and non-immune related cell lines. The MFI of ssDNA was set as 1, and the ratio to the MFI of ssDNA is expressed. Results are expressed as the mean + SD of three determinations. Data are representative of three independent experiments.

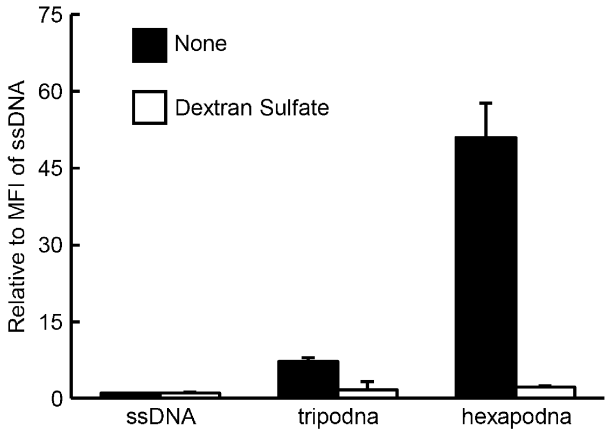

Figure 19. Uptake of nanostructured DNAs in RAW264.7 cells. The MFI of ssDNA was set as 1, and the ratio to the MFI of ssDNA is expressed. Results are expressed as the mean + SD of four determinations.
Data are representative of two independent experiments.

Cellular uptake of Alexa Fluor 488-labeled ssDNA, tripodna, and hexapodna was examined in various cell lines. Figure 18 shows the MFI value of cells after addition of Alexa Fluor 488-labeled DNA samples. The MFI values of RAW264.7 and DC2.4 cells after addition of Alexa Fluor 488-tripodna or Alexa Fluor 488-hexapodna were significantly higher than those observed after addition of Alexa Fluor 488-ssDNA. In contrast, the MFI values of NIH3T3, MAEC, and C166 cells were low irrespective of the DNA samples added. These results indicate that the hexapodna structure itself, not the additional ODNs, is important for efficient uptake of Alexa Fluor 488-labeled DNA in RAW264.7 and DC2.4 cells. Figure 19 shows the MFI value of RAW264.7 cells pretreated with DS prior to the addition of Alexa Fluor 488-labeled ssDNA, tripodna, and hexapodna. DS significantly reduced the cellular uptake of Alexa Fluor 488-tripodna and Alexa Fluor 488-hexapodna.

I-3-3-b. Cellular uptake of nanostructured DNA among various immune/non-immune cells

Figure 20 shows the MFI of Alexa Fluor 488-labeled tetrapodna, tetrahedron, or tetragon. The results in RAW264.7 cells and DC2.4 cells are similar to previous studies[25,38]. On the other hand, the MFI value was hardly induced by structuring DNA in non-immune cells. These results suggest that nanostructured DNA are more efficiently taken up by immune cells than non-immune cells.

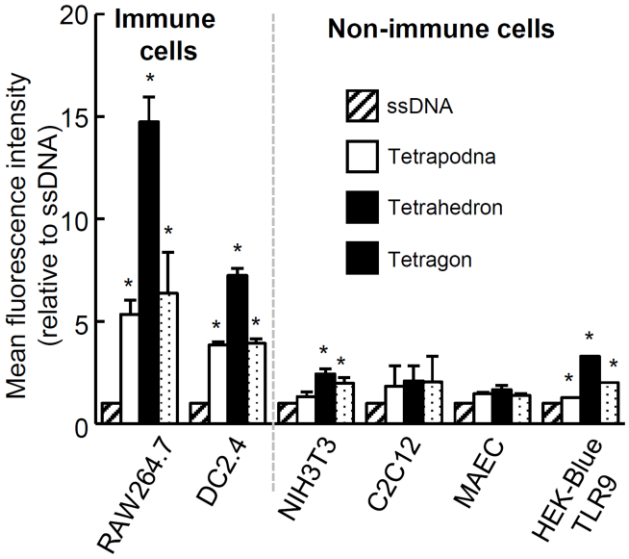

Figure 20. Uptake of ssDNA, tetrapodna, tetrahedron, and tetragon in immune and non-immune related cell lines. The MFI of ssDNA was set as 1, and the ratio to the MFI of ssDNA is expressed. Results are expressed as the mean + SD (n=4). *$p < 0.05$ compared with ssDNA group.

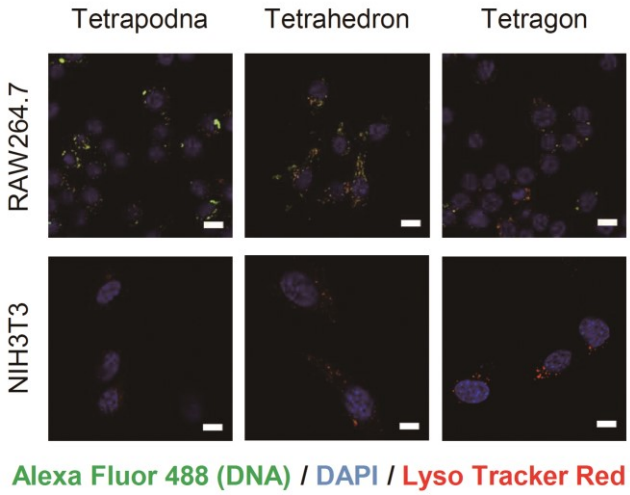

Figure 21. Florescent images were observed using confocal fluorescence microscopy. Scale bars, 10 μm.

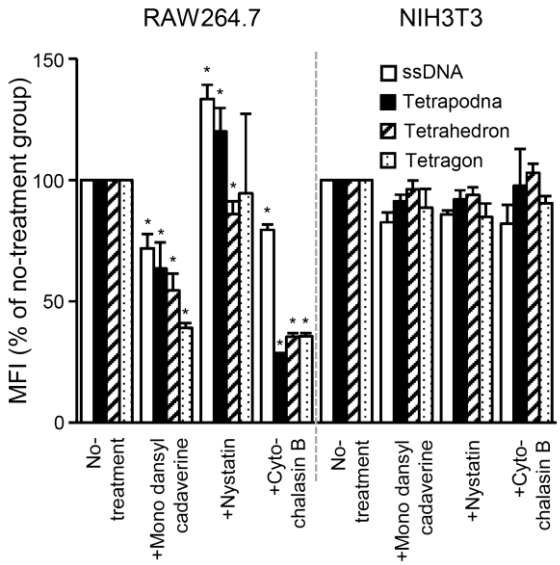

Figure 22. RAW264.7 cells and NIH3T3 cells were incubated with non, 100 μM mono dansyl cadaverine, 100 μg/mL nystatin, or 15 μ g/mL cytochalasin B for 30 min, then treated with ssDNA, tetrapodna, tetrahedron, or tetragon. Results are expressed as mean + SD. *$p < 0.05$ compared with the no-treatment groups.

I-3-3-c. Internalization of nanostructured DNA into RAW264.7 cells

Figure 21 shows the confocal microscopy images of RAW264.7 cells or NIH3T3 cells cells at 2 h after the addition of Alexa Fluor 488-labeled tetrapodna, tetrahedron, or tetragon. In RAW264.7 cells, all DNA samples co-localized with lyso tracker red. On the other hand, the fluorescence signal of Alexa Fluor-488 was hardly observed in NIH3T3 cells. These results indicate that nanostructured DNA was internalized into immune cells such as RAW264.7 cells via endocytosis pathway.

I-3-3-d. Uptake pathways of nanostructured DNA

Figure 22 shows the MFI value of Alexa Fluor 488-labeled tetrapodna, tetrahedron, or tetragon. The MFI value of RAW264.7 cells treated with mono dancyl cadaverine or cytochalasin B were critically reduced compared with no-treatment group. This result indicates that clathrin-mediated endocytosis is involved in the uptake of nanostructured DNA by RAW264.7 cells.

I-3-4 Discussion

For clinical use of nucleic acid drugs, it is necessary to consider the uptake by various types of cells, including immune cell and non-immune cells. Several reports suggested that nanostructured DNAs are useful for the delivery of nucleic acid to immune cells. In this section, I selected RAW264.7 cells and DC2.4 cells as immune cells, and MAEC cells, C166 cells, NIH3T3 cells, C2C12 cells, and HEK-Blue hTLR9 cells as non-immune cells. In Figure 18 and 20, nanostructured DNAs were more efficiently taken up by immune cells than by non-immune cells. This result suggested that nanostructured DNAs have potential of selective delivery of nucleic acids to immune cells.

Clathrin-mediated endocytosis, an well-known endocytic pathways, is caused by ligand binding to cell surface receptors, and endosomal vesicles formed by clathrin are taken up by cells[45–47]. Results shown in Figure 22 suggested that nanostructured DNAs were efficiently taken up by RAW264.7 cells via clathrin-mediated endocytosis, and they were hardly taken up via endocytic pathways by NIH3T3 cells.

There are two general intracellular pathways for uptake of nanosized molecules. Large molecules than 250 nm are taken up by cells via phagocytosis, and small molecules are taken up via pinocytosis[48]. Pinocytosis includes micropinocytosis, clathrin-mediated endocytosis, caveolae-mediated endocytosis, and clathrin-/caveolae-independent endocytosis[49]. In phagocytosis pathway and micropinocytosis pathway, nanosized molecules taken up by cells are transferred directly to the lysosome, while molecules taken up by cells via clathrin-mediated endocytosis are transported to endosome. In present study, nanosized structured CpG DNAs were effectively recognized by endosomal TLR9. These strongly suggest that clathrin-mediated endocytosis would be involved in cellular uptake of nanostructured DNAs. However, further investigation about endocytic receptors is required.

Taken together, uptake of nanostructured DNAs in immune cell was more efficient than non-immune cells, and calthrin-mediated endocytosis was involved in the uptake process of nanostructured DNAs in RAW264.7 cells.

Chapter II

Design of DNA-based delivery systems to immune cells using DNA origami or DNA supramolecules

The results in Chapter I suggest that tetrahedral DNA or bend DNA could efficiently interact with immune cells, while there is little information about the relationship between structural properties of nanostructured DNA and cellular uptake. Then, I hypothesized that the structural rigidity and compactness of nanostructured DNAs would be a key for their interaction with immune cells. In Chapter II, I used two experimental methods to elucidate involvement of structural rigidity or structural compactness in cellular uptake of nanostructured DNA by immune cells.

In Section 1, I used DNA origami technology to elucidate the involvement of structural rigidity in the cellular uptake of nanostructured DNA. DNA origami technology is useful for create nanoscale shapes and patterns. Then, I designed various rectangular DNAs with varying numbers of staple strands. Rectangular DNA with fewer staples could have more structural flexibility than rectangular DNA with full staples. The cellular uptake of these nanostructured DNAs was evaluated.

In Section 2, DNA supramolecules formed by hydrophobic interaction were designed. To elucidate the involvement of structural compactness, I designed RCA products and cholesterol modified RCA products with different compactness.

In this chapter, the results are presented in the following two sections.

Chapter II

Section 1

Folding of single-stranded circular DNA into rigid rectangular DNA origami accelerates its cellular uptake

II-1-1 Introduction

The self-assembling nature of DNA has been used to construct uniquely-structured DNA nanostructures, including immobile Holliday junctions and cubic cages[50,51]. The DNA origami technology, in which a long single-stranded 'scaffold' DNA and many short 'staple' DNAs complementary to parts of the scaffold DNA are used, has created precisely-designed, two- or three-dimensional DNA nanostructures with sophisticated functions[17,52,53]. These DNA origami-based nanostructures have been applied as sensors for single nucleotide polymorphism (SNP) and RNA sequences[54,55].

Therapeutic applications of such nanostructures have also been explored, because DNA is a biologically active compound. Previous studies from my laboratory reported that DNA nanostructures consisting of three or more oligodeoxynucleotides (ODNs) were efficiently taken up by immune cells, including mouse macrophage-like RAW264.7 cells and mouse bone marrow-derived dendritic cells. When these DNA nanostructures contained the immunostimulatory unmethylated cytosine-phosphate-guanine (CpG) DNA, they efficiently induced the release of proinflammatory cytokines from these immune cells expressing Toll-like receptor 9, the intracellular receptor for CpG DNA[24,25,38,56]. This enhanced cytokine release was demonstrated to be effective in inhibiting tumor growth in tumor-bearing mouse models[57,58].

It was also found that the increased activity of CpG DNA by constructing DNA nanostructures was attributed to the increased cellular uptake. I demonstrated that the uptake of single-stranded, double-stranded, and branched, polypod-like structured DNAs was dependent on their structural complexity[24]. Another study using tetrapod-like structured DNA (tetrapodna), tetrahedral DNA (tetrahedron), and tetragonal DNA (tetragon), all of which were prepared using four ODNs of the same length, also showed that the uptake of these DNA nanostructures by RAW264.7 cells was quite different from one another[38]. These differences in the cellular uptake would be related to their structural properties. Although there is little information about the relationship between the structural properties and cellular uptake of DNA nanostructures, it can be speculated, based on their possible structural flexibility, that tetrahedron may be more rigid than the others. This difference in flexibility may lead to differences in their cellular uptake.

To prove this hypothesis, DNA nanostructures with similar shape but different flexibility are preferable. The DNA origami technology can be used to construct a series of DNA nanostructures with appropriate structural properties. In the present section, a rectangular DNA (RecDNA) was designed with a scaffold DNA

and 50 staples, and ones with fewer staples were also prepared as more flexible ones. The cellular uptake of these DNA nanostructures was evaluated after addition to RAW264.7 cells.

II-1-2 Materials and Methods

Chemicals

All chemicals were of the highest grade available and used without further purification as described in Chapter I, Section 1.

Cell culture

RAW264.7 cells were cultured as described in Chapter I, Section 1. Cells were then seeded on 96-well culture plates at a density of 5×10^5 cells/well and cultured for 24 h prior to use.

Scaffold

Firstly, a 1800 bp sequence of pCpG-mcs plasmid (InvivoGen) was amplified by polymerase chain reaction using the following primers: the forward primer: 5′-ACTTCTAGATACAAATGTGGTATGGAATTCAGTC-3′, the reverse primer: 5′-CATTCTAGACCTCAGCGAAACAGAGAGCTGAACAAAGAG-3′. The underline shows the position of the recognition site of Xba I, bold shows the recognition site of Nt.BbvcI. The both ends of the PCR product were digested with Xba I (Takara Bio), ligated using a DNA ligation kit ver.2.1 (Takara Bio). GT115 strain Escherichia coli was transformed with the double -strand circular DNA obtained and Miniprep was performed for amplification, then the double- strand circular DNA was purified using GenElute Plasmid Miniprep Kit (Sigama-Aldrich). It was sequenced three times using a BigDye Terminator v3.1 Cycle Sequencing Kit (Thermo Fisher Scientific Inc.) by ABI3000xl (Thermo Fisher Scientific Inc.) using the following primers: primer 1: 5′-GGAATTCAGTCAATATGTTCAC-3′ primer 2: 5′-AGAGAATTGTAATATGCAGATTAT-3′ primer 3: 5′-GCAACTGTGTGCACTTTGTG-3′. Maxiprep was performed to obtain sufficient amount of double -strand DNA, and it was purified by a PureLink HiPure Plasmid Maxiprep Kit (Thermo Fisher Scientific Inc.). The one strand of double- strand DNA was digested with nicking endonuclease Nt.BbvCI (New England BioLabs, Ipswich, MA, USA), subsequently the nicked strand was digested with Exonuclease III (New England BioLabs). The formation of scaffold was analyzed by agarose gel electrophoresis and the scaffold of purpose was extracted from the gel, and purified by NucleoSpin Gel and PCR Clean-up (Takara Bio). The sequences of the scaffold are listed in Table 4.

Staples

Staples, short DNA with length of 24-40 base, were purchased from Eurofin Genomics Japan K.K. (Tokyo, Japan). The sequences of the staples of RecDNA are listed in Table 5. Each staple was identified with a code like 0[68]-1[52] according to the following rule: the helix (0) and base ([68]) numbers of the position of its 5′-end and

the helix (1) and base ([52]) numbers of the position of its 3′-end. Four ODNs labeled with Alexa Fluor488 at the 5′-end were purchased from Japan BioService Co.,Ltd. (Saitama, Japan)

Preparation of DNA nanostructure

Each structure was prepared by mixing equimolar amounts of scaffold and staples. In brief, scaffold and staples dissolved in an annealing buffer (20 mM Tris-HCl, 1 mM ethylenediaminetetraacetic acid (EDTA), and 10 mM magnesium chloride, pH 7.3) were mixed at a final concentration of 60 nM for each DNA. The mixtures were then heated to 85°C and cooled down to 35°C at -0.2 °C /min, cooled to 20°C at -1 °C/min, then gradually cooled to 4°C using a thermal cycler (PC-818S Program Temp Control System; ASTEC Co., Ltd., Fukuoka, Japan). The products were analyzed at 4°C by agarose gel electrophoresis in 0.5 × TBE buffer (45 mM Tris borate, 1 mM EDTA, supplemented with 11 mM $MgCl_2$), stained with SYBR Gold and observed using a LAS3000 (Fujifilm, Tokyo, Japan). To determine the amount of fluorescent-labeled staples incorporated into each structure, the fluorescence of Alexa Fluor488-labeled staples were imaged after agarose gel electrophoresis, using a LAS3000 with excitation wave length 460 nm. The size of each DNA nanostructure was measured by dynamic light scattering (DLS) using Zetasizer Nano ZS (Malvern, Worcestershire, UK)

AFM imaging of DNA nanostructures

Atomic force microscopy (AFM) images of each structure were obtained on a AFM system (Nano Live Vision, RIBM, Tsukuba, Japan) using a silicon nitride cantilever (BL-AC10EGS; Olympus, Tokyo, Japan). In brief, a DNA sample was adsorbed on a freshly cleaved mica plate pretreated with 0.1% aqueous 3-aminopropyltriethoxysilane for 5 min at room temperature and then washed three times with a buffer solution containing 20 mM Tris and 10 mM $MgCl_2$. Scanning was performed in the same buffer solution.

Confocal fluorescence microscopic observation

Alexa Fluor488-labeled single stranded DNA (ssDNA), each rectangular DNA, or Scaffold4 at 9 nM in 200 μL of Opti-MEM was added to RAW264.7 cells on 8-well slide chamber at a density of 5 × 10^5 cells/mL for confocal fluorescence microscopy and incubated for 4 h at 37°C. RAW264.7 cells were washed with phosphate buffer saline (PBS) twice, fixed with 4% paraformaldehyde for 20 min, and washed twice with PBS. To stain nuclei, the cells were treated by 4′, 6-diamino-2-phenylindole (DAPI) and incubated for 5 min, and washed once with PBS. Then, the cells were coverslipped with SlowFade Gold (Life Technologies, Tokyo, Japan), and observed using a confocal fluorescence microscope (Nikon A1R MP, Nikon, Tokyo, Japan).

Flow cytometry

Alexa Fluor488-labeled single stranded DNA (ssDNA), each rectangular DNA, or Scaffold4 at 5.5 nM in 50 μL Opti-MEM was added to RAW264.7 cells on 96 well plate at a density of 5 × 10^5 cells/mL for flow

cytometry and incubated for 4 h at 37°C. RAW264.7 cells were washed three times with PBS and harvested. Then, the fluorescence intensity of cells was determined by flow cytometry (Gallios Flow Cytometer, BD Biosciences, NJ, USA) using Kaluza software (version 1.0, BD Biosciences), and the mean fluorescence intensity (MFI) was calculated.

Statistical analysis

Differences were statistically evaluated by one-way analysis of variance (ANOVA) followed by the Tukey-Kramer test for multiple comparisons. A P value of < 0.05 was considered statistically significant.

Table 4. The sequences of the scaffold.

CTAGATACAAATGTGGTATGGAATTCAGTCAATATGTTCACCCCAAAAAAGCTGTTTGTTAACTTGCCAACCTCATTC
TAAAATGTATATAGAAGCCCAAAAGACAATAACAAAAATATTCTTGTAGAACAAAATGGGAAAGAATGTTCCACTA
AATATCAAGATTTAGAGCAAAGCATGAGATGTGTGGGGATAGACAGTGAGGCTGATAAAATAGAGTAGAGCTCAGA
AACAGACCCATTGATATATGTAAGTGACCTATGAAAAAAATATGGCATTTTACAATGGGAAAATGATGATCTTTTTC
TTTTTTAGAAAAACAGGGAAATATATTTATATGTAAAAAATAAAAGGGAACCCATATGTCATACCATACACACAAA
AAAATTCCAGTGAATTATAAGTCTAAATGGAGAAGGCAAAACTTTAAATCTTTTAGAAAATAATATAGAAGCATGC
CATCAAGACTTCAGTGTAGAGAAAAATTTCTTATGACTCAAAGTCCTAACCACAAAGAAAAGATTGTTAATTAGATT
GCATGAATATTAAGACTTATTTTTAAAATTAAAAAACCATTAAGAAAAGTCAGGCCATAGAATGACAGAAAATATTT
GCAACACCCCAGTAAAGAGAATTGTAATATGCAGATTATAAAAAGAAGTCTTACAAATCAGTAAAAAATAAAACTA
GACAAAAATTTGAACAGATGAAAGAGAAACTCTAAATAATCATTACACATGAGAAACTCAATCTCAGAAATCAGAG
AACTATCATTGCATATACACTAAATTAGAGAAATATTAAAAGGCTAAGTAACATCTGTGGCTTAATTAAAACAGGTA
GTTGACAATTAAACATTGGCATAGTATATCTGCATAGTATAATACAACTCACTATAGGAGGGCCATCATGGCCAAGT
TGACCAGTGCTGTCCCAGTGCTCACAGCCAGGGATGTGGCTGGAGCTGTTGAGTTCTGGACTGACAGGTTGGGGTTC
TCCAGAGATTTTGTGGAGGATGACTTTGCAGGTGTGGTCAGAGATGATGTCACCCTGTTCATCTCAGCAGTCCAGGA
CCAGGTGGTGCCTGACAACACCCTGGCTTGGGTGTGGGTGAGAGGACTGGATGAGCTGTATGCTGAGTGGAGTGAG
GTGGTCTCCACCAACTTCAGGGATGCCAGTGGCCCTGCCATGACAGAGATTGGAGAGCAGCCCTGGGGGAGAGAGT
TTGCCCTGAGAGACCCAGCAGGCAACTGTGTGCACTTTGTGGCAGAGGAGCAGGACTGAGGATAACCTAGGAAACC
TTAAAACCTTTAAAAGCCTTATATATTCTTTTTTTTCTTATAAAACTTAAAACCTTAGAGGCTATTTAAGTTGCTGATT
TATATTAATTTTATTGTTCAAACATGAGAGCTTAGTACATGAAACATGAGAGCTTAGTACATTAGCCATGAGAGCTT
AGTACATTAGCCATGAGGGTTTAGTTCATTAAACATGAGAGCTTAGTACATTAAACATGAGAGCTTAGTACATACTA
TCAACAGGTTGAACTGCTGATCTTAATTAAAATTATCTCTAAGGCATGTGAACTGGCTGTCTTGGTTTTCATCTGTAC
TTCATCTGCTACCTCTGTGACCTGAAACATATTTATAATTCCATTAAGCTGTGCATATGATAGATTTATCATATGTATT
TTCCTTAAAGGATTTTTGTAAGAACTAATTGAATTGATACCTGTAAAGTCTTTATCACACTACCCAATAAATAATAAA
TCTCTTTGTTCAGCTCTCTGTTTCGCTGAGGT

Table 5. The sequences of staples of RecDNA.

Name	Sequences (5′ → 3′)
0[68]1[52]	**TTTTGGGGTGAACATATTGACTGAGAGATTTA**
0[100]1[84]	**TAGAATGAGGTTGGCAAGTTAACAGACTTTAC**
***0[132]0[101]**	**TGTTATTGTCTTTTGGGCTTCTATATACATTT**
0[164]1[148]	**TTCTTTCCCATTTTGTTCTACAAGTCTGTTTC**
0[188]1[180]	**TAAATCTTGATATTTACTCACTGT**
1[53]3[52]	**TTATTTATGCTTAATGGAATTATACAGCCAGT**
1[85]3[84]	**AGGTATCAAAAATACATATGATAAATTAAGAT**
1[117]2[101]	**AGGTCACTTGTAAAATGCCATATTCAAAAATC**

1[149]3[148]	**TGAGCTCTTCTAAAAAAGAAAAAGTCTCCATT**
1[181]3[180]	**CTATCCCCATTTTTTACATATAAATTTTGTGT**
2[36]0[29]	**TCAGGTCACAGAGAGCTGAACAAAATTCCATACCACATTT**
2[68]0[69]	**TATGCACATGGGTAGTGTGATAAAAACAGCTT**
2[100]1[116]	**CTTTAAGGATTCAATTAGTTCTTATTTTTCAT**
2[132]0[133]	**TTTCCCATTACATATATCAATGGGAATATTTT**
2[164]0[165]	**CCTGTTTTACTCTATTTTATCAGCGTGGAACA**
3[53]5[52]	**TCACATGCCTAAACCCTCATGGCTAAGCTCTC**
3[85]5[84]	**CAGCAGTTGTTTAATGTACTAAGCAAATCAGC**
3[117]4[101]	**TCTAAAAGTGATGGCATGCTTCTATGTACTAA**
3[149]5[148]	**TAGACTTAGTCATAAGAAATTTTTCTATGGCC**
3[181]5[180]	**GTATGGTATAACAATCTTTTCTTTTTTTAAAA**
4[36]2[37]	**AAGCTCTCCAGATGAAAACCAAGAAATATGTT**
4[68]2[69]	**TTAATGAACTTAGAGATAATTTTAATCTATCA**
4[100]3[116]	**GCTCTCATCAACCTGTTGATAGTATATTATTT**
4[132]2[133]	**TGAAGTCTATTTAAAGTTTTGCCTATCATCAT**
4[164]2[165]	**GACTTTGATAATTCACTGGAATTTTATATTTC**
5[53]7[52]	**ATGTTTGAGGTTTCCTAGGTTATCCAGGGCAA**
5[85]7[84]	**AACTTAAAAAAAGAATATATAAGGCAATCTCT**
5[117]6[101]	**GTGTTGCACATATTACAATTCTCTAAGTTTTA**
5[149]7[148]	**TGACTTTTTACTGATTTGTAAGACCAATGATA**
5[181]7[180]	**ATAAGTCTATCTGTTCAAATTTTTTTCTCATG**
6[36]4[37]	**TGCTCCTCTCATGTTTCATGTACTAATGTACT**
6[68]4[69]	**GGTTTTAAACAATAAAATTAATATTCTCATGT**
6[100]5[116]	**TAAGAAAATAGCCTCTAAGGTTTTTTACTGGG**
6[132]4[133]	**ATAATCTGAATATTTTCTGTCATTCTCTACAC**
6[164]4[165]	**TTATTTTTCTTAATGGTTTTTTAAGTGGTTAG**
7[53]9[52]	**ACTCTCTCAGTCCTCTCACCCACACAGGGTGA**
7[85]9[84]	**GTCATGGCCCACCTCACTCCACTCAGTCATCC**
7[117]8[101]	**TATTTCTCCACAGATGTTACTTAGCTGAAGTT**
7[149]9[148]	**GTTCTCTGGTTTAATTGTCAACTACACATCCC**
7[181]9[188]	**TGTAATGATGTATTATACTATGCATGGTCACTTGGCCAT**
8[36]6[37]	**AGGGTGTTTGCCTGCTGGGTCTCTCTCAGTCC**
8[68]6[69]	**GCTCATCCCCCCAGGGCTGCTCTCCTTTTAAA**

8[100]7[116]	**GGTGGAGAAGGGCCACTGGCATCCCCTTTTAA**
8[132]6[133]	**AATTAAGCTAATTTAGTGTATATGTTCTTTTT**
8[164]6[165]	**ATGCCAATATTTCTGAGATTGAGTGTCTAGTT**
***9[53]8[69]**	**CATCATCTCTGACCACACCTGCAAAGCATACA**
***9[85]9[116]**	**TCCACAAAATCTCTGGAGAACCCCAACCTGTC**
9[117]8[133]	**AGTCCAGAACTCAACAGCTCCAGCCCTGTTTT**
***9[149]8[165]**	**TGGCTGTGAGCACTGGGACAGCACGATATACT**
9[29] 8[37]	**GGACTGCTGAGATGAACCCAAGCC**

All ODNs have a phosphodiester backbone. Modification of Alexa Fluor-488 indicated by asterisk (*).

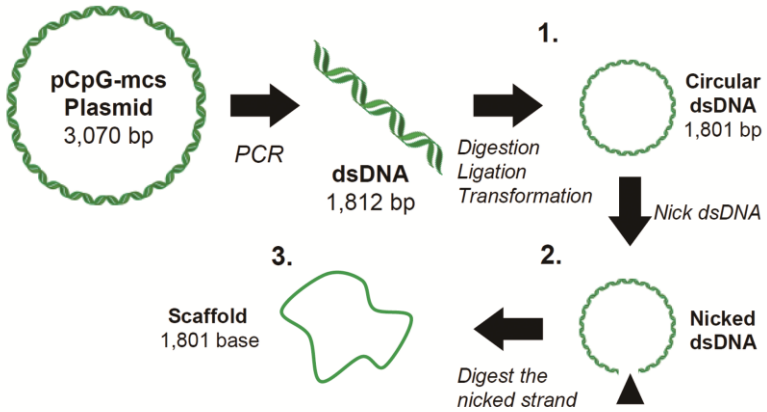

Figure 23. Schematic overview of scaffold preparation. 1812 bp sequence of pCpG-mcs plasmid DNA amplified by PCR. (1.) Both ends of the PCR product were digested by XbaI, ligated by T4 nuclease, then transformed into Esherichia coli. (2.) Obtained doubled strand circular DNA was nicked by nicking endonuclease Nt.BbvCI. (3.) The nicked strand was digested by exonucleaseIII to obtain scaffold.

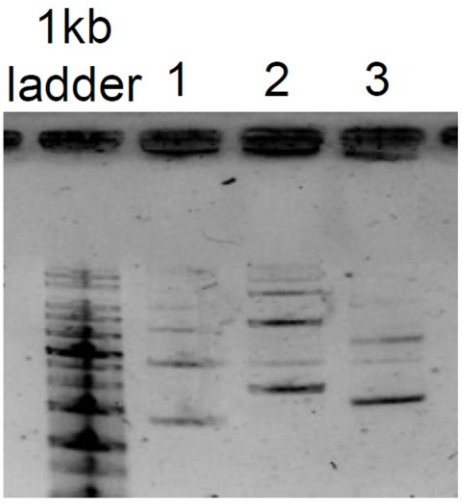

Figure 24. Agarose gel electrophoresis analysis of scaffold preparation. lane1, circular double strand DNA; lane2, nicked double strand DNA; lane3 scaffold.

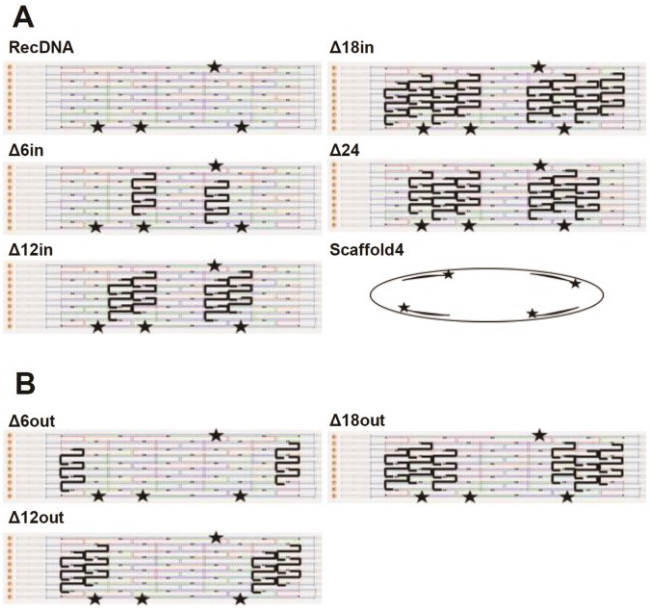

Figure 25. (A) Six, twelve, eighteen or twenty-four staples located close to the center of RecDNA were removed to obtain Δ6in, Δ12in, Δ18in, and Δ24, respectively (Δ(n)in). The star indicates the Alexa Fluor-488 conjugated to the 5′-end of staple. The bold staples are the missing staples. (B) Six, twelve or eighteen staples located close to the edges of RecDNA were removed to prepare Δ6out, Δ12out, and Δ18out, respectively (Δ(n)out).

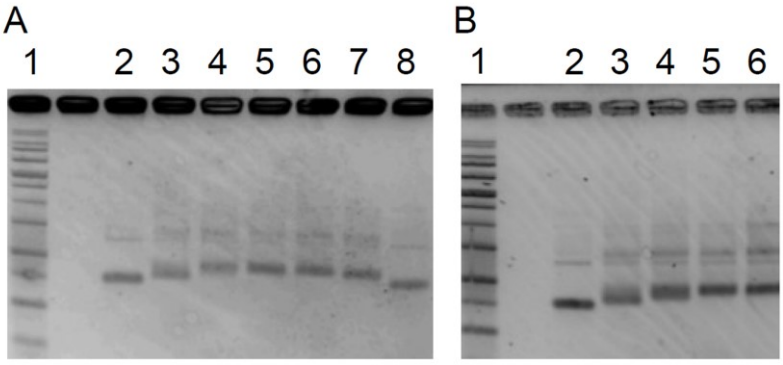

Figure 26. Agarose gel electrophoresis analysis of assembled DNA origami. A, lane1, 1kbp DNA ladder; lane2, scaffold; lane3, RecDNA; lane4, Δ6in; lane5, Δ12in; lane6, Δ18in; lane7, Δ24; lane8, Scaffold4. B, lane1, 1kbp DNA ladder; lane2, scaffold; lane3, RecDNA; lane4, Δ6out; lane5, Δ12out; lane6, Δ18out.

II-1-3 Results

II-1-3-a. Formation of scaffold

Figure 23 shows the schematic overview of the scaffold preparation. The sequence analysis of the double strand circular DNA after ligation of the PCR product revealed that there was one base substitution (T to C at position 67) and one base (G) insertion at position 840 (data not shown). The double strand circular DNA with these mutations was used to prepare scaffold. Figure 24 shows the agarose gel electrophoresis analysis of circular double strand DNA, nicked double strand DNA, and scaffold. The band shift after the treatment of each recognition enzyme suggests the formation of scaffold. Although there were several bands, the band with the

highest mobility was considered to be the scaffold of purpose from its molecular weight, excised from the gel, purified, and used as scaffold in the following experiments.

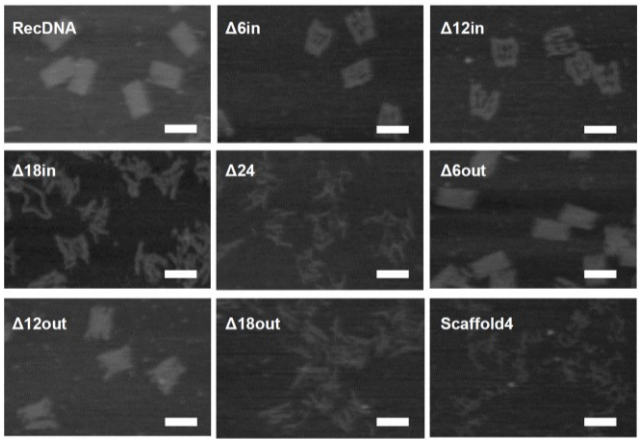

Figure 27. AFM images of RecDNA, Δ(n)in, Δ(n)out, Scaffold4. Scale bar, 50 nm.

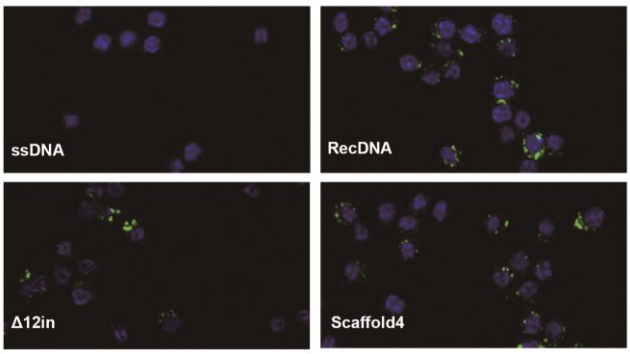

Figure 28. Cellular uptake of Alexa-Fluor488-labeled ssDNA, RecDNA, Δ12in, Scaffold4 at final concentration 9nM observed by confocal microscopy.

II-1-3-b. Formation of rectangular DNAs

Schematic images of RecDNA, Δ (n)in, Δ (n)out, Scaffold4 were drawn in Figure 25. Figure 26 shows the agarose gel electrophoresis analysis of each structure. All preparations had a major single band, indicating each structure was successfully formed with high yield. Figure 27 shows the AFM image of each structure. The image of RecDNA shows a rectangular shape with expected size. As the staples were removed, the shape became unraveled. These results of electrophoresis and AFM imaging indicate that all the DNA nanostructures were formed as designed.

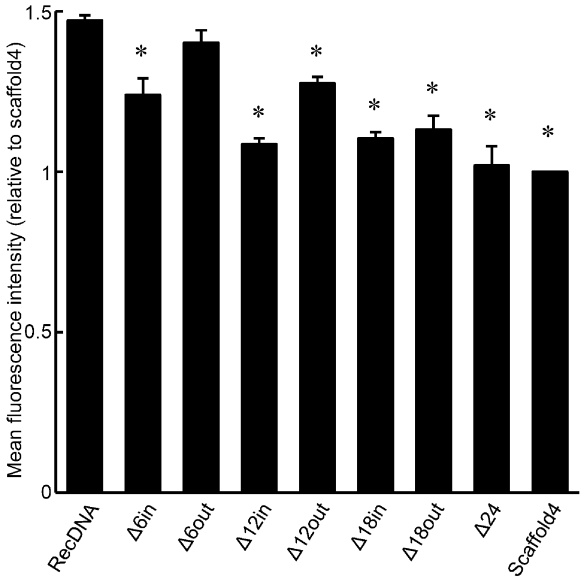

Figure 29. Cellular uptake of Alexa-Fluor488-labeled DNA nanostructures at final concentration 5.5 nM. Results are expressed as the ratio of MFI of four wells relative to Scaffold4. *$p < 0.05$ vs RecDNA.

II-1-3-c. Properties of each structure

In fluorescence imaging analysis, the migration distance of Alexa Fluor488-labeled staples shows the staples were annealed properly to all the structures (data not shown). The size of RecDNA, (n)in, (n)out were around 30 nm, suggesting structures with similar size were prepared. Scaffold4, one hardly folded, was around 500 nm. (data not shown)

II-1-3-d. Uptakes by RAW264.7 cells

Figure 28 shows confocal microscopic images of ssDNA, RecDNA, Δ12in, Scaffold4. The images showed that all the structures were efficiently taken up by RAW264.7 cells compared to ssDNA.

II-1-3-e. Influence of removal of inside or outside staples of RecDNA on cellular uptake

Figure 29 shows the ratio of each MFI of RAW264.7 cells relative to that of Scaffold4 after addition of Alexa Fluor488-labeled RecDNA, Δ(n)in, Δ(n)out, and Scaffold4. The cellular uptake of RecDNA was the highest, and the removal of the staples reduced the uptake. Removal of the outside staples had less pronounced effects on the uptake than removal of the inside ones.

II-1-4 Discussion

Most studies on DNA origami use M13mp18 single stranded DNA of 7249 bases as scaffold, because the source of a long single stranded DNA other than this is limited. Several approaches have been explored to overcome this limitation[59,60]. Taking into consideration that the upper size limit of endocytosis is around 100 nm[61], shorter single stranded DNAs can be suitable as a scaffold to evaluate the relationship between the structural properties and cellular uptake of DNA nanostructures. DNA nanostructures consisting of three to eight ODNs were about 10 nm in diameter and up to 300 bases per unit. Therefore, I designed and constructed a new scaffold of 1800 bases, and developed rectangular DNA with height of 24.5 nm and width of 54.1 nm. The size of this rectangular DNA was a little larger than those of ODN-based DNA nanostructures, but was comparable to the size of nanosized drug delivery systems, such as polymeric micelles and liposomes.

CpG DNA is an immunostimulatory CpG motif-containing DNA and expected to be an adjuvant in the treatment of cancer and infectious diseases. Rectangular DNA or other DNA-origami-based DNA nanostructures containing CpG motifs can be easily prepared by using CpG DNA-containing template, such as pcDNA3.1 plasmid. However, a preliminary study in my laboratory showed that the presence of CpG DNA in DNA nanostructures increased their uptake by immune cells, such as RAW264.7 cells compared to ones without CpGs. Cells stimulated with CpG DNA would secrete proinflammatory cytokines, and then accelerate the cellular uptake of DNA nanostructures. To avoid this, pCpG-mcs, a CpG-free plasmid was used as the template for the preparation of CpG-free scaffold. However, the yield of scaffold preparation was not high (50μg / 340μg), so the method for the preparation of the scaffold needs further improvements.

In this section, cellular uptake was highest in RecDNA, and DNA nanostructures with fewer staples, which are probably more flexible, showed lower uptake. In addition, the cellular uptake decreased more when inside staples were removed than when outside ones were removed. This suggests that the positions of single and double stranded DNA in the structure affect the interaction with cells. In addition, the loops on the both sides of the structure may lessen the change of its structure by removing outside staples. These findings suggest that structural properties, probably its flexibility, affect the cellular uptake, which is consistent with the hypothesis of this study.

The uptake of RecDNA was about 1.5 times higher than that of Scaffold4. The difference was not so great compared with those observed in the previous studies using ODNs in Chapter I, Section 1. The reason why the difference was so small would be due to the large size of the DNA nanostructures used in this study compared with those of the ODN-based DNA nanostructures. Another possible reason is the difference between 2D and 3D

structures. While this study focused on the cellular uptake of a series of 2D DNA nanostructures with different flexibility, the previous one studied on 3D DNA nanostructures, tetrapodna, tetrahedron, and tetragon, which may have different 3D structural flexibility such as range of motion. Therefore, further studies with DNA nanostructure of different 3D structural flexibility may have more remarkable effect on the cellular uptake. Bent DNA nanostructures can be easily designed by using DNA origami, and further studies using such DNA nanostructures would provide additional information on the relationship between the structural properties and cellular uptake of DNA nanostructures.

In conclusion, the present section showed that the cellular uptake of RecDNA, the rectangular DNA with full staples, was more efficient than DNA nanostructure with fewer staples Δ(n)in, Δ(n)out, Scaffold4. In addition, the effect on the decrease of cellular uptake was larger by removing inside staples than outside staples. These results will provide useful information for the development of optimal DNA nanostructure for cellular uptake toward DNA nanostructure-based delivery systems for nucleic acid medicines.

Chapter II

Section 2

Development of DNA supramolecules formed by hydrophobic interaction for the effective delivery of CpG DNA

II-2-1 Introduction

My laboratory previously reported that various DNA nanostructures can be prepared using three or more oligodeoxynucleotides (ODNs). The DNA nanostructures were efficiently taken up by mouse macrophage-like RAW264.7 cells, and increased the immunostimulatory activity of CpG DNA. Therefore, DNA nanostructures can be used to efficiently deliver CpG DNA to immune cells[22,24,38].

In Chapter I, Section1, I revealed that tetrahedral DNA showed the most efficient interaction with immune cells. In Chapter II, Section 1, I also concluded that rectangular DNAs with many staples were more efficiently taken up by RAW264.7 cells. It could be because of their structural compactness.

Self-assembled polymer amphiphiles consisting of hydrophilic and hydrophobic segments are attractive materials because of their potential application in drug delivery[62,63]. For example, pullulan, which is an exo-polysaccharide produced by yeast like fungus Aureobasidium pullulans, is a water soluble, non-toxic and biocompatible polymer[64]. It has been demonstrated that pullulan modified with cholesterol forms self-assembled nanogel particles in water and that these nanoparticles act as a good drug carrier because of high drug-loading and cell-targeting capacity[65–67].

Rolling circle amplification (RCA) is a simple and efficient isothermal enzymatic process in which a circularized template DNA is amplified by DNA polymerase. RCA is able to produce long single stranded DNA (ssDNA) composed of multiple tandem repeats that are complementary to a circular DNA template[68,69]. In this section, I tried to prepare amphiphilic DNA supramolecules composed of CpG DNA-containing RCA products added with hydrophobic segments for the efficient delivery of CpG DNA. Figure 30 summarizes the scheme for the preparation of the DNA supramolecules. In brief, a long ssDNA containing CpG DNA is amplified by RCA using the circular DNA template and the RCA products are complementarily annealed with a short length DNA modified with cholesterol (chol-DNA) to form supramolecules based on hydrophobic interaction. It was supposed that RCA products annealed with chol-DNA, DNA supramolecules, had more compact structure than RCA products. It was evaluated whether RCA products annealed with chol-DNA could form supramolecules. Moreover, it was investigated whether the uptake of CpG DNA by immune cells and immunostimulatory activity of CpG DNA could be improved by the formation of such DNA supramolecules.

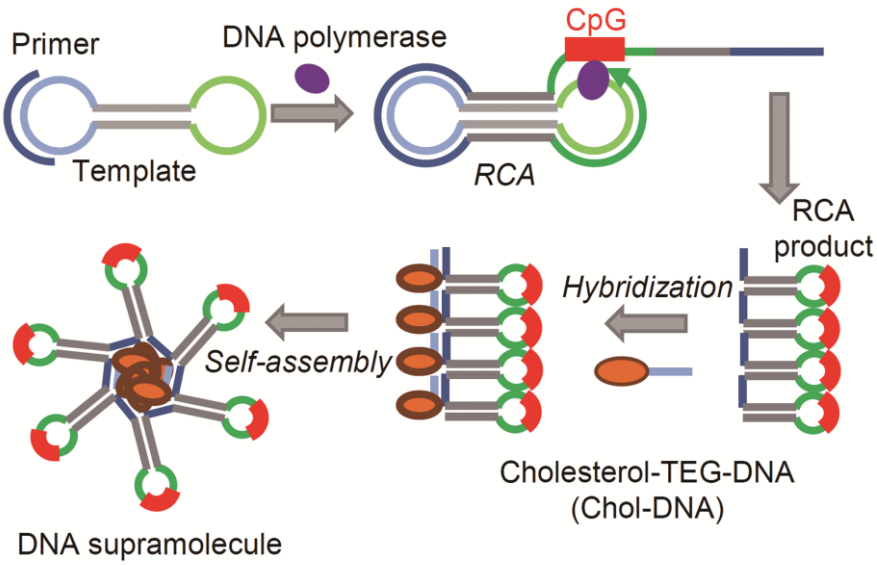

Figure 30. The design of hydrophobic DNA supramolecules containing CpG DNA.

II-2-2 Materials and Methods

Chemicals

All chemicals were the highest grade available and used without further purification as described in Chapter I, Section 1.

Cell culture

RAW264.7 cells were cultured as described in Chapter I, Section 1. Cells were plated on 96-well culture plates at a density of 5×10^4 cells/well and cultured for 24 h prior to use.

Oligodeoxynucleotides

RCA primer and CpG1668 were obtained from Fasmac (Kagawa, Japan), and the other ODNs were obtained from Integrated DNA Technologies, Inc.. Sequences of the ODNs used are shown in Table 6.

Preparation of Template ODNs

ODNs were dissolved in an annealing buffer (10 mM Tris-HCl (pH 8), 1 mM ethylenediaminetetraacetic acid (EDTA), and 200 mM NaCl). Template ODN (100 μM) was self-annealed by heating at 95°C for 5 min followed by gradual cooling down to 20°C using a thermal cycler (PC-818S Program Temp Control System; ASTEC Co., Ltd., Fukuoka, Japan). The annealed template was ligated at 16°C for 4 h in solution containing 10 U/μL T4 DNA ligase (Takara Bio), 66 mM Tris-HCl (pH 7.6), 6.6 mM $MgCl_2$, 10 mM dithiothreitol (DTT), and 0.1 mM ATP to prepare circularized templates. Circularized linear oligonucleotides were removed by reaction with 25 U/mL exonuclease I (Takara Bio) and 1000 U/mL exonuclease III (Takara Bio) at 37°C for 30 min.

RCA products preparation

Equivalent molar amounts of the circularized template and RCA primer were mixed together and were annealed by heating at 95°C for 5 min followed by gradual cooling down to 20°C. The resultant mixture (1.25 μM) was subjected to RCA by incubating at 30°C for 16 h in a solution containing 0.4 U/μL Phi29 DNA polymerase (Lucigen, WI, USA), 50 mM Tris-HCl (pH 7.5), 10 mM $MgCl_2$, 10 mM (NH4)2SO4, 4 mM DTT, 200 μg/ml BSA, and 2 mM each dNTP (Invitrogen, Carlsbad, CA, USA). Cy5-labled RCA product was prepared by performing RCA under the above condition with 10 μM Cy5-dCTP (GE Healthcare UK Ltd., England). RCA products containing CpG motifs (RCA_{pro}) was amplified using template 1 and RCA products without CpG motifs (RCA_{pro} (non CpG)) was amplified using template 2.

Preparation of DNA supramolecules

The highly viscous RCA products were incubated in 5 mM EDTA (Sigma-Aldrich) at 80°C for 15 min to solubilize the product. After purification by 300 kDa Pall Nanosep® centrifugal devices (Nippon Genetics, Tokyo, Japan) with water, chol-DNA (Integrated DNA Technologies, Inc.) was added to the purified RCA products and they were annealed by heating at 95°C for 5 min followed by gradual cooling down to 20°C in an annealing buffer described above. RCA_{pro}-chol was composed of RCA_{pro} and chol-DNA, and RCA_{pro} (non CpG)-chol was composed of RCA_{pro} (non CpG) and chol-DNA.

Oligodeoxynucleotide analysis

DNA products in each step were analyzed by polyacrylamide electrophoresis (PAGE) or alkaline agarose gel electrophoresis. PAGE was carried out with 12% acrylamide under 250 V for 30 min at 4°C, and alkaline agarose gel electrophoresis was carried out with 0.8% agarose in 50mM NaOH and 1 mM EDTA under 30 V for 4 h.

Dynamic light scattering analysis

The apparent sizes of the RCA product and RCA products annealed with chol-DNA were determined by the dynamic light scattering analysis using a Malvern Zetasizer 3000HS (Malvern Instruments, Malvern, UK) at 20°C. The measurement was repeated more than five times, and the results are expressed as the mean ± S.D. of the five measurements.

Transmission electron microscope (TEM) observation

To observe the structure, RCA_{pro} or RCA_{pro}-chol was mixed with an equal volume of 4% paraformaldehyde. This mixture was subsequently applied to a carbon/formvar film-coated TEM grid (Alliance Biosystems, Osaka, Japan) and incubated for 20 min. The sample was then washed with phosphate-buffered saline (PBS) and fixed with 1% glutaraldehyde for 5 min. After another wash with PBS, the sample was incubated with 1% uranyl

acetate for 3 min. The sample was observed under a TEM (Hitachi H-7650; Hitachi High-Technologies Corporation, Tokyo, Japan).

Cellular uptake of DNA

RAW264.7 cells seeded on 96-well plates were incubated with Cy5-labeled RCA_{pro} or RCA_{pro}-chol in 100 μL of Opti-MEM for 2 h at 37°C. Cells were then washed three times with 200 μL of PBS and harvested. Then, the fluorescence intensity of cells was determined by flow cytometry (Gallios Flow Cytometer). The mean fluorescence intensity (MFI) was calculated by using Kaluza software.

TNF-α release from RAW264.7 cells

CpG1668, RCA_{pro}, RCA_{pro}-chol, RCA_{pro} (non CpG)-chol or chol-DNA was diluted in 100 μL of Opti-MEM and added to RAW264.7 cells seeded in 96-well plates. The cells were incubated at 37°C for 8 h, and the supernatants were retrieved and stored at −80°C until use. TNF-α concentration in the supernatants were determined by enzyme-linked immunosorbent assay (ELISA) using OptEIA™ sets (BD Biosciences).

Statistical analysis

Statistical comparisons were performed by Student's t test for two groups. Statistical differences were considered when the *P* value was < 0.05.

Table 6. The sequences of ODNs.

Name	Sequences (5′ → 3′)	Length (mer)
Template 1	5′-phosphate-GTCATCAGCCAAACATTACAGCTTGCTACA GGCTGATGACCTGTCAAGATAGCATCAGGAACGTCATG GAATCTTGACAG-3′	80
Template 2 (nonCpG)	5′-phosphate-GTCATCAGCCAAACATTACAGCTTGCTACA GGCTGATGACCTGTCAAGATTCCATGACGTTCCTGATG CTATCTTGACAG-3′	80
RCA primer	5′-CAGCCTGTAGCAAGCTGTAATGTTTGGCTG-3′	30
Chol-DNA	5′-AAACATTACAGCTTGCTACA-TEG-Cholesterol-3′	20
CpG1668	5′-TCCATGACGTTCCTGATGCT-3′	20

Underlined in Template 1 is the complementary sequences to the murine CpG motif (AACGTC) and in CpG1668 is the CpG motif (GACGTT). Abbreviations: TEG, triethylene glycol.

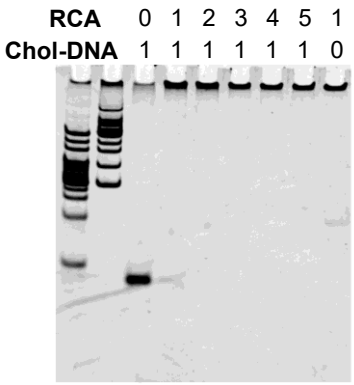

Figure 31. Electrophoretic analysis of RCA products. RCA products were annealed with chol-DNA at indicated ratio and analyzed by 12% PAGE.

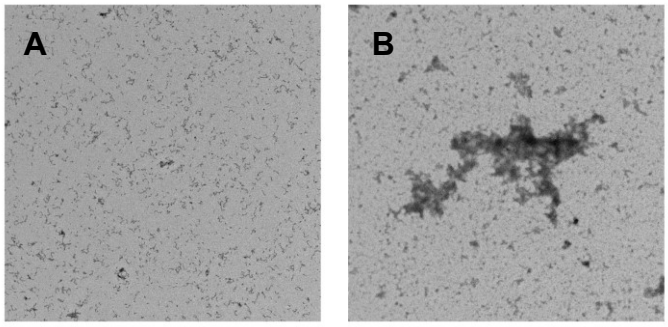

Figure 32. TEM images of RCA_{pro} (A) and RCA_{pro}-chol (B).

II-2-3 Results

II-2-3-a. Preparation of DNA supramolecules

To prepare RCA products, RCA was performed with a circularized template DNA annealed with RCA primer. The electrophoretic analysis showed that long ssDNAs were amplified by RCA. An average base length of RCA products estimated by measuring absorbance at 260 nm was approximately 16,000 bases, which seems to be in agreement with the base length estimated by electrophoretic analysis.

Then, different amounts of RCA products were hybridized with chol-DNA which was complementary to RCA products. The electrophoretic analysis indicated that the band of chol-DNA alone remained at the ratio of hybridization site in RCA products: chol-DNA = 1 : 1, and disappear at the ratio of 2:1. Therefore, not all of the hybridization sites in RCA products were hybridized with chol-DNA (Figure 31). Considering from the disappearance of chol-DNA alone band in the PAGE analysis, approximately one out of three hybridization sites in the RCA products were hybridized with chol-DNAs.

The dynamic light scattering studies demonstrated that the apparent size of RCA products varied widely (762 ± 590 nm). On the other hand, apparent size of RCA products hybridized with chol-DNA was 144 ± 49 nm. Figure 32 shows TEM images of RCA_{pro} and RCA_{pro}-chol. While long single strands were observed in RCA_{pro} samples, formation of supramolecules was observed in RCA_{pro}-chol samples.

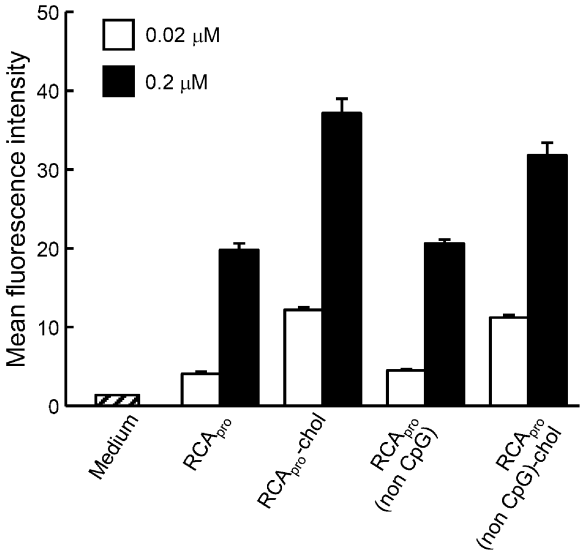

Figure 33. Cellular uptake of Cy5-labeled RCA_{pro} and RCA_{pro}-chol (with or without CpG) at a final concentration of 0.1 or 0.2 μM CpG motifs. Results are expressed as mean + S.D. of four wells. * $P<0.05$ vs RCA_{pro} at the same concentrations.

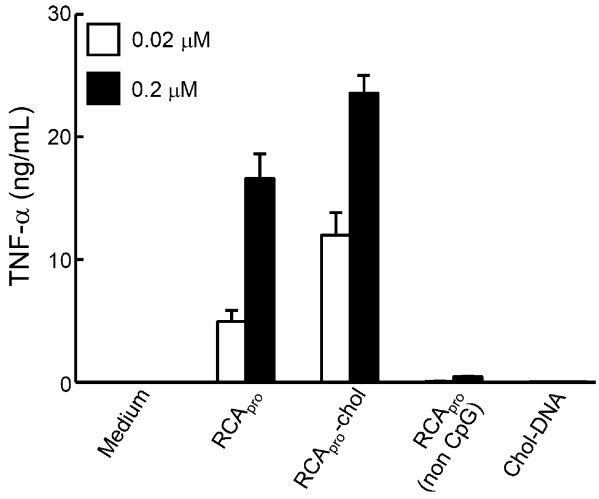

Figure 34. TNF-α release by RAW264.7 cells after added each DNAs at a final concentration of 0.1 or 0.2 μM CpG DNA. Results are expressed as mean +S.D of four wells. * $P<0.05$ vs RCA_{pro} at the same concentration.

II-2-3-b. Cellular uptake of Cy5-labeled RCA_{pro}-chol in RAW264.7 cells

Figure 33 shows the MFI of RAW264.7 cells after addition of Cy5-labbeled DNA samples. RAW264.7 cells added with Cy5-labeled RCA_{pro}-chol showed significantly higher MFI values than that of the cells added with Cy5-labeled RCA_{pro}.

II-2-3-c. TNF-α release from RAW264.7 cells after addition of RCA_{pro}-chol containing CpG motifs

The immunostimulatory activity of the DNA supramolecules was examined using mouse macrophage-like RAW264.7 cells. Figure 34 shows the amount of TNF-α release from RAW264.7 cells after addition of CpG1668, RCA_{pro}, RCA_{pro}-chol, or RCA_{pro} (non CpG)-chol. Compared with CpG1668, RCA_{pro} induced more TNF-α release from RAW264.7 cells. Moreover, compared with RCA_{pro}, RCA_{pro}-chol induced significantly more TNF-α release from RAW264.7 cells.

II-2-4 Discussion

In this section, I developed CpG DNA delivery carrier composed of RCA products and complementary chol-DNAs. RCA products were hybridized with chol-DNA via DNA-DNA base pairing and formed the supramolecules probably because of hydrophobic cholesterol groups. Two out of hybridization sites for chol-DNA in RCA products seemed not to be hybridized with chol-DNA probably due to the steric hindrance of cholesterol groups on DNAs.

Flow cytometry analysis showed that the uptake of Cy-5 RCA products in immune cells, mouse macrophage-like RAW264.7 cells, was increased by hybridization with chol-DNA. Moreover, the DNA supramolecules possessed high potency to induce TNF-α release from RAW264.7 cells probably due to increase

in uptake. As it was shown that the uptake of non-modified liposomes by rat alveolar macrophages increased with an increase in particle size over the range of 100-1000 nm[70], the large size RCA products might be more efficiently taken up by RAW264.7 cells than CpG1668 to induce more TNF-α release. Furthermore, it was also demonstrated that the particle shape is important for the cellular uptake. Spherical particles showed higher uptake by macrophages compared with non-spherical particles[71]. Therefore, more efficient uptake of RCA_{pro}-chol by RAW264.7 cells than RCA_{pro} may be due to the difference in the shape because TEM observation revealed that RCA_{pro}-chol showed more spherical shape than RCA and RCA_{pro}.

RCA is a simple and efficient isothermal enzymatic process to generate long single stranded DNA (ssDNA). By designing the template, the RCA products can include functional sequences including DNA aptamers, DNAzymes, and spacer domains[72]. Thus, various templates permit a synthesis of versatile supramolecules.

CpG DNA is effective as immune adjuvants, and the co-delivery of antigens with CpG DNA adjuvant enhances the immunogenicity of the antigen compared to the separate delivery[73–75]. Moreover, amphiphilic polymer-based nanoparticles can encapsulate lipophilic antigens into their inner cores[76,77]. Therefore, the DNA supramolecules that can load antigens by the hydrophobic interaction are potential antigen delivery carriers that may be able to induce strong immune response through efficient co-delivery of antigens with CpG DNA.

In conclusion, the present section shows that RCA_{pro}-chol formed supramolecules delivered CpG DNA to RAW264.7 cells and enhanced the immunostimulatory activity of CpG DNA. Considering the facts that RCA_{pro}-chol was more compact than RCA_{pro} (Figure 32) and that RCA_{pro}-chol was more efficiently taken up by RAW264.7 cells than RCA_{pro} was, structural compactness could be a key for their interaction with immune cells.

Chapter III

Elucidation of cell surface receptors involved in the cellular uptake of nanostructured DNA

III-1 Introduction

Various classes of nucleic acid drugs are being marketed or under development. Attention must be paid to toxicity issues during the development of nucleic acid drugs[78]. Nucleic acid drug candidates have several toxicity issues, including off-target effects, immune stimulation, hematoxicity, hepatotoxicity, and nephrotoxicity. Immune stimulation occurs when toll-like receptors (TLRs) recognize DNA or RNA. Several reports have suggested that certain small interfering RNA molecules cause immune stimulation via TLRs[79–85]. Therefore, it is clearly important to evaluate unexpected TLR-mediated immune stimulation in the development of nucleic acid drug candidates.

TLR9 is the only TLR that recognizes DNA. Its ligand is a DNA molecule containing an unmethylated cytosine–phosphate–guanine (CpG) motif, i.e., CpG DNA. Because bacterial and viral DNAs contain many CpG motifs, TLR9-mediated responses form part of the self-defense system against the invasion of such pathogens[7,86,87]. TLR9 is expressed in the endosomes of various mammalian cells, including plasmacytoid dendritic cells and B-cells[88]. After cellular uptake and sorting into endosomes, CpG DNA binds to TLR9 and induces the release of proinflammatory cytokines, which then activate innate immunity[10,89]. It is expected that such responses can be exploited to treat cancer, infection, and allergic diseases[11,12]. I have previously reported that nano-construction of CpG DNA is a unique and promising method of increasing the immunostimulatory activity of CpG DNA[38]. Studies using a series of polypod-like structured DNAs demonstrated that the cellular uptake of CpG DNA was significantly increased by its incorporation into nanostructured DNAs[24,25,56]. However, the mechanisms involving the structure-dependent uptake of DNA require further elucidation. To develop efficient delivery systems, interaction of nanostructured DNA and immune cells needs to be elucidated and optimized.

The endosomal localization of TLR9 indicates that membrane protein(s) other than TLR9 are responsible for the cellular uptake of DNA. So far, several DNA receptors have been reported. These include macrophage scavenger receptor-1 (MSR1, SR-A, and CD204), αMβ2 (MAC-1), advanced glycosylation end product-specific receptor (AGER), membrane-associated nucleic acid-binding protein (MNAB), mannose receptor-1 (MRC1), and lymphocyte antigen 75 (DEC-205)[35,36,90–93]. However, in most cases their contribution to DNA uptake has been examined using phosphorothioate (PS) DNA, which non-specifically binds to cell membranes more strongly than natural phosphodiester (PO) DNA. The results obtained with PS DNA cannot be used to estimate the contribution of DNA receptors in the cellular responses to nucleic acid drug candidates. Msr1, which mediates the endocytosis of negatively charged molecules such as acetylated low-density lipoprotein (LDL) and oxidized LDL, is reportedly involved in the uptake of PO DNA by macrophages[90]. Therefore, Msr1-mediated DNA uptake could be involved in TLR-mediated immune stimulation by nucleic acid drug candidates.

HEK-Blue TLR cells are commercially available and can be used for the analysis of the immunological properties of various TLR ligands[94]. HEK-Blue hTLR9 cells respond to PS CpG DNA and release secreted embryonic alkaline phosphatase (SEAP)[95]. However, my preliminary studies have shown that PO CpG DNA induces very little SEAP release from HEK-Blue hTLR9 cells. Because HEK293 cells, which constitute the parent

cell line of HEK-Blue TLR9 cells, are non-immune cells, they do not express any DNA receptors on their cell membranes. Therefore, I hypothesized that low cellular uptake of CpG DNA by HEK-Blue hTLR9 cells might explain the weak or absent response to PO CpG DNA. Therefore, in the present chapter, I sought to establish cell lines that respond to both PS and PO CpG DNAs. Such cells would be useful for the screening of nucleic acid drug candidates with diverse physicochemical properties.

I revealed that nanosized DNA assemblies are useful for delivery of nucleic acid drugs to immune cells in Chapter I and Chapter II. I also elucidated that structural rigidity or structural compactness could be a key for efficient delivery of nucleic acid drugs to immune cells via cellular uptake receptor. Then, I also hypothesized that HEK-Blue hTLR9 cells expressing cell surface receptor candidates is useful for elucidate the involvement in cellular uptake of nanostructured DNA to immune cells.

To this end, I transduced HEK-Blue hTLR9 cells with human hMSR1 to obtain HEK-Blue hTLR9/hMSR1 cells in the hope that the transfection of the *MSR1* gene to HEK-Blue hTLR9 cells would increase the uptake of PO DNA. I first evaluated the effect of transfection of the *MSR1* gene on the cellular uptake of DNA. I then determined whether HEK-Blue hTLR9/hMSR1 cells respond to both PS and PO CpG DNAs. I selected phosphorothioate CpG2006 (PS CpG2006), a single-stranded PO CpG DNA (ssCpG), and a tetrapod-like structured DNA containing the ssCpG (tetraCpG) as model TLR9 ligands. HEK-Blue hTLR9 cells and HEK-Blue hTLR7 cells were also used for the analysis of cellular responses to CpG DNA.

III-2 Materials and Methods

Chemicals

Dulbecco′s modified Eagle′s medium (DMEM) was obtained from Nissui Pharmaceutical, Co., Ltd. (Tokyo, Japan). Sodium chloride, sodium hydrogen phosphate, sodium bicarbonate, potassium chloride, glucose, sodium dodecyl sulfate (SDS) methanol, and WIDE-VIEW Prestained Protein Size Marker III were purchased from Wako Pure Chemicals Industries, Ltd. (Osaka, Japan). Tris was obtained from Nacalai Tesque (Kyoto, Japan). Blasticidin, zeocin, normocin, CL264, and HEK-Blue detection reagents were purchased from InvivoGen (San Diego, CA, USA). Opti-modified Eagle′s medium (Opti-MEM) and fetal bovine serum (FBS) were obtained from Thermo Fisher Scientific Inc. (Waltham, MA, USA). A 100-base pair (bp) DNA ladder was purchased from Takara Bio (Otsu, Japan). All other chemicals were of the highest grade available and were used without further purification.

Cell culture

HEK-Blue hTLR7 and HEK-Blue hTLR9 cells were obtained from InvivoGen. The cells were cultured in DMEM supplemented with 10% heat-inactivated FBS, 0.2% sodium bicarbonate, 100 IU/mL penicillin, 100 μg/mL streptomycin, 2 mM L-glutamine, 10 mg/mL blasticidin, 100 mg/mL zeocin, and 50 mg/mL normocin at 37°C in humidified air containing 5% CO_2 as per the manufacturer’s instructions.

Plasmid DNA

Plasmid pcDNA3.1 was purchased from Thermo Fisher Scientific Inc. A plasmid vector encoding human macrophage scavenger receptor-1 (human MSR1, hSR-A, hCD204) was constructed by insertion of the FLAG-tagged MSR1 fragment amplified by polymerase chain reaction (PCR) from a cDNA clone of human MSR1 (GE Healthcare UK Ltd., Buckinghamshire, England) into the multi-cloning site of pcDNA3.1.

Transfection of hMSR1-expressing plasmid DNA in HEK-Blue Cells

HEK-Blue hTLR7 and HEK-Blue hTLR9 cells were cultured in 75-cm^2 tissue culture flasks, and were transfected with a pcDNA3.1 vector encoding MSR1 or an empty pcDNA3.1 vector using Lipofectamine 2000 (Thermo Fisher Scientific Inc.) according to the manufacturer's instructions. After 20 h of incubation, the cells were used as HEK-Blue hTLR7/hMSR1 and HEK-Blue hTLR9/hMSR1 cells. The cells transfected with empty pcDNA3.1 vector were used as mock controls.

Western blotting of hMSR1 in HEK-Blue hTLR cells

The cells were lysed in a lysis buffer (PicaGene Dual Sea Pansy Luminescence Kit, Toyo Ink, Tokyo, Japan), and the cell lysates were reduced by the addition of dithiothreitol to 100 mM. A fraction of the cell lysate (7 μg protein) was subjected to 10% SDS-polyacrylamide gel electrophoresis (PAGE) and transferred to a polyvinylidene fluoride transfer membrane (Immobilon-P; Merck Millipore Ltd, Darmstadt, Germany). The membrane was then blocked in Blocking One (Nacalai Tesque, Kyoto, Japan). The membrane was incubated with anti-hMSR1 antibody (R&D Systems, Minneapolis, MN, USA) for 1 h at 20–22°C. The membrane was then incubated with horseradish peroxidase (HRP)-conjugated rabbit anti-mouse IgG antibody (Thermo Fisher Scientific Inc.) for 1 h at room temperature. Protein bands were detected by chemiluminescence using an Immobilon Western chemiluminescent HRP substrate (Merck Millipore, Billerica, MA, USA).

Confocal microscopic detection of hMSR1 in HEK-Blue cells transduced with hMSR1

Untreated, mock-transfected, or *MSR1*-transfected HEK-Blue hTLR9 cells were seeded on a chamber slide at a density of 3×10^4 cells/well and then cultured for 24 h. The cells were washed twice with phosphate-buffered saline (PBS), fixed with 4% paraformaldehyde for 20 min, and washed again twice with PBS. The cells were then blocked with 20% FBS in PBS for 1 h. The cells were incubated with anti-FLAG M2 antibody (Sigma-Aldrich, St. Louis, MO, USA) and 10% FBS in PBS for 1 h at room temperature, and then washed once. The cells were incubated with Alexa Fluor 488-labeled anti-mouse IgG antibody (Abcam Plc, Cambridge, UK) for 1 h at room temperature, and washed once. The cells were incubated with 600 nM 4′,6-diamidino-2-phenylindole (DAPI; Life Technologies) for 5 min at room temperature and washed once. The chamber was then removed and the slide was observed using a confocal microscope (A1R MP, Nikon Instech Co., Ltd., Tokyo, Japan) as previously reported[44].

Oligodeoxynucleotides

All oligodeoxynucleotides (ODNs) used were purchased from Integrated DNA Technologies, Inc. (Coralville, IA, USA). The sequences of the ODNs used are presented in Table 7. Phosphodiester ODN-3-1, which contained a potent human CpG motif (GTCGTT), was used as single-stranded CpG DNA (ssCpG). ssCpG and three other phosphodiester ODNs were dissolved in an annealing buffer (TE buffer, 10 mM Tris-HCl, pH 8, 1 mM ethylenediaminetetraacetic acid, and 150 mM sodium chloride) and mixed in sterile water to produce a final concentration of 100 μM for each ODN. The mixtures were then incubated at 95°C for 5 min and slowly cooled to 4°C using a thermal cycler to obtain tetrapodna containing ssCpG (tetraCpG). Phosphorothioate CpG2006 (PS CpG2006), a single-stranded B-type CpG DNA, was used as a positive control to induce SEAP release from the HEK-Blue hTLR9 cells. For cellular uptake experiments, ODN-3-1 labeled with Alexa Fluor 488 at the 5′ end was purchased from Japan BioService Co., Ltd. (Saitama, Japan). Each sample was analyzed at room temperature by 6% PAGE. The DNA bands were visualized using SYBR Gold (Molecular Probes, Eugene OR, USA).

Uptake of DNA in HEK-Blue cells

Untreated, mock-transfected, or *MSR1*-transfected HEK-Blue hTLR9 cells were seeded onto 48-well plates at a density of 1×10^5 cells/well. Alexa Fluor 488-ssCpG or Alexa Fluor 488-tetraCpG diluted with 0.1 mL of Opti-MEM was then added to the cells. After 2 h incubation at 37°C, the cells were washed three times with 400 μL of PBS and harvested. The fluorescence intensity of the cells was then determined by flow cytometry (Gallios Flow Cytometer; Beckman Coulter, Inc., CA, USA) using Kaluza software (version 1.0; Beckman Coulter), and the mean fluorescence intensity (MFI) was calculated. Similar experiments were carried out on the untreated, mock-transfected, and HEK-Blue hTLR7 cells.

SEAP release from HEK-Blue cells

The untreated, mock-transfected, or *MSR1*-transfected HEK-Blue hTLR9 cells were seeded onto 96-well plates at a density of 5×10^4 cells/well. PS CpG2006, ssCpG, or tetraCpG in HEK-Blue detection solution was added to the cells to produce a final concentration of 50 μg/mL. After 20 h incubation at 37°C, the optical density (OD) of the samples was measured at a wavelength of 620 nm using a microplate reader. Similar experiments were carried out on untreated, mock-transfected, and HEK-Blue hTLR7 cells.

Inhibition of DNA uptake in HEK-Blue cells by anti-hMSR1 antibody

The untreated, mock-transfected, or *MSR1*-transfected HEK-Blue hTLR9 cells were seeded onto 48-well plates at a density of 1×10^5 cells/well. The cells were pretreated with anti-hMSR1 antibody or IgG1 isotype control (R&D Systems, Minneapolis, MN, USA) at a concentration of 2 μg/mL for 1 h. After washing, the cells were treated with 2 μg/mL Alexa Fluor 488-ssCpG or Alexa Fluor 488-tetraCpG diluted with 0.1 mL of Opti-MEM together with anti-hMSR1 antibody or IgG1 isotype control to produce a final concentration of 2

μg/mL. After 2 h incubation at 37°C, the cells were washed three times with 400 μL of PBS and harvested. The fluorescence intensity of the cells was determined by flow cytometry using Kaluza software, and the MFIs were calculated.

Statistical analysis

Differences were evaluated statistically by one-way analysis of variance (ANOVA), followed by the Tukey–Kramer test for multiple comparisons and the Student's t-test for two groups. $P < 0.05$ values were considered statistically significant.

Table 7. The sequences of the oligodeoxynucleotides (ODNs) for the DNA nanostructures.

Name	Sequences (5′ → 3′)	Length (mer)
ODN-1	TCGTCGTTTTGTCGTTTTGTCGTTTACATTCCTAAGTCTGA AACATTACAGCTTGCTACACGAGAAGAGCCGCCATAGTA	80
ODN-1′	TACTATGGCGGCTCTTCTCGTGTAGCAAGCTGTAATGTTT CAGACTTAGGAATGT	55
tetrapodna-2	TTACTATGGCGGCTCTTCTCGTGTAGCATAGTGTCGTTTTA TCACCAGGCAGTTG	55
tetrapodna-3	TCAACTGCCTGGTGATAAAACGACACTACGTGGGAATCTT GACAGGTCATCAGCC	55
tetrapodna-4	TGGCTGATGACCTGTCAAGATTCCCACGAGCTGTAATGTT TCAGACTTAGGAATG	55
PS CpG2006	T*C*G*T*C*G*T*T*T*T*G*T*C*G*T*T*T*T*G*T*C*G*T*T	24

All ODNs have a phosphodiester backbone. The asterisks (*) indicate the positions of phosphorothioate (PS) modifications. The CpG motif (GTCGTT) is underlined.

III-3 Results

III-3-a. Establishment of HEK-Blue hTLR9/hMSR-1 cells

Figure 35A shows the results of western blotting analysis of the cell lysates using anti-hMSR1 antibody. The lysate of HEK-Blue hTLR9/hMSR1 cells revealed a band of approximately 75 kDa, which corresponded to the FLAG-tagged hMSR1. The band was not detected in the lysates of the untreated or mock-transfected HEK-Blue hTLR9 cells, indicating that FLAG-tagged hMSR1 was expressed in the HEK-Blue hTLR9/hMSR1 cells. I examined the localization of hMSR1 in the HEK-Blue hTLR9 cells using confocal microscopy. Figure 35B presents confocal microscopy images of untreated, mock-transfected, and MSR1-transfected HEK-Blue hTLR9 cells. The Alexa Fluor 488-labeled anti-FLAG antibody was bound to the cell surface of the HEK-Blue

hTLR9/hMSR1 cells. However, there was little fluorescence in the untreated or mock-transfected cells. These results indicate that hMSR1 localizes at the cell surface of the HEK-Blue hTLR9/hMSR1 cells.

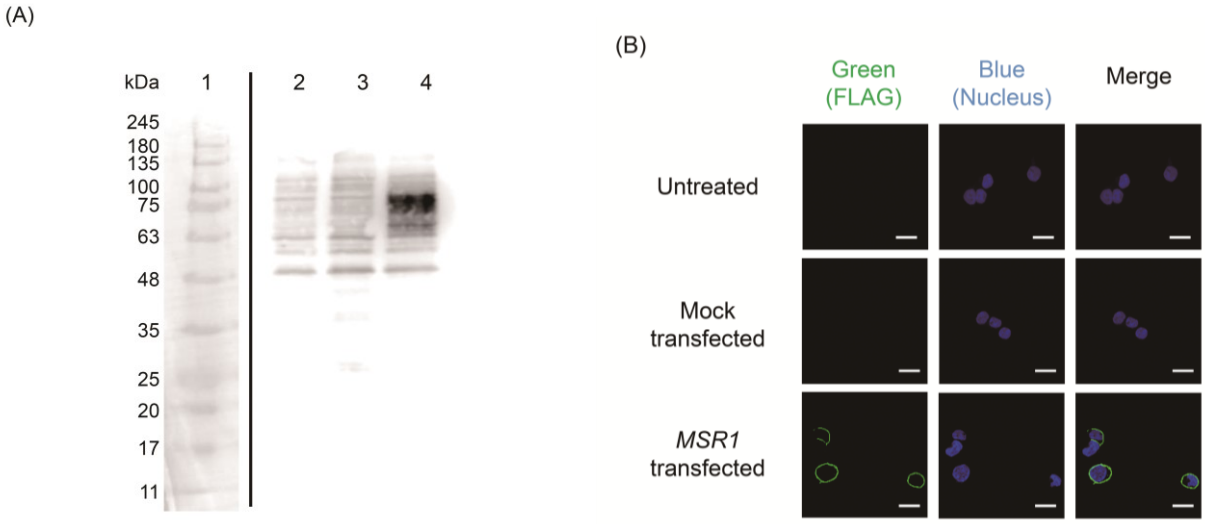

Figure 35. Confirmation of hMSR1 expression in HEK-Blue hTLR9 cells. (A) hMSR-1 protein was detected by western blotting using anti-hMSR1 antibody. Bright field (lane 1) and chemiluminescence (lanes 2-4) images were shown. Lane 1, protein size marker; lane 2, untreated HEK-Blue hTLR9 cells; lane 3, mock-transfected HEK-Blue hTLR9 cells; lane 4, HEK-Blue hTLR9/hMSR1 cells. (B) Confocal microscopy images of untreated, mock-transfected, or *MSR1*-transfected HEK-Blue hTLR9 cells immunostained with anti-FLAG antibody and Alexa Fluor-488 conjugated anti-mouse IgG1 antibody. Scale bar, 20 μm.

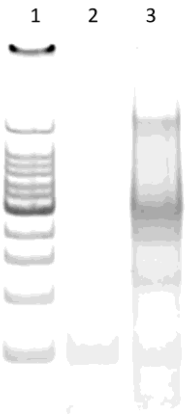

Figure 36. Electrophoretic analysis of ssCpG and tetraCpG. Aliquots of ssCpG and tetraCpG were run on 6% PAGE at room temperature. Lane 1, 100 bp ladder; lane 2, ssCpG; lane 3, tetraCpG.

III-3-b. Evaluation of the functions of HEK-Blue hTLR9/hMSR-1 cells

Figure 36 shows the results of the PAGE analysis of ssCpG and tetraCpG prepared at a DNA concentration of 100 μM. ssCpG and tetraCpG are represented by single PAGE bands, indicating that tetraCpG had been prepared with high efficiency.

Figure 37 shows the MFI of the HEK-Blue hTLR9 cells, the mock-transfected HEK-Blue hTLR9 cells, and the HEK-Blue hTLR9/hMSR1 cells after the addition of Alexa Fluor 488-labeled DNA samples. The MFI values of the HEK-Blue hTLR9/hMSR1 cells were significantly higher than those of the mock-transfected HEK-Blue hTLR9 cells after addition of Alexa Fluor 488-ssCpG or tetraCpG. There was no significant difference in the MFI value of the HEK-Blue hTLR9/hMSR1 cells between Alexa Fluor 488-ssCpG and tetraCpG. In contrast, the MFI values of the cells after addition of Alexa Fluor 488-PS CpG2006 were not significantly different among the cells, irrespective of hMSR1 expression (data not shown).

Figure 38 shows SEAP activity after the addition of PS CpG2006, ssCpG, and tetraCpG. The HEK-Blue hTLR9 cells or mock-transfected HEK-Blue hTLR9 cells released SEAP upon the addition of PS CpG2006, but

did not release SEAP after the addition of ssCpG or tetraCpG. However, PS CpG2006, ssCpG, and tetraCpG all induced SEAP release from the HEK-Blue hTLR9/hMSR1 cells. There was no significant difference in SEAP activity after the addition of PS CpG2006 among the three types of cells. The SEAP activities of the HEK-Blue hTLR9/hMSR1 cells were comparable in both ssCpG and tetraCpG treatments.

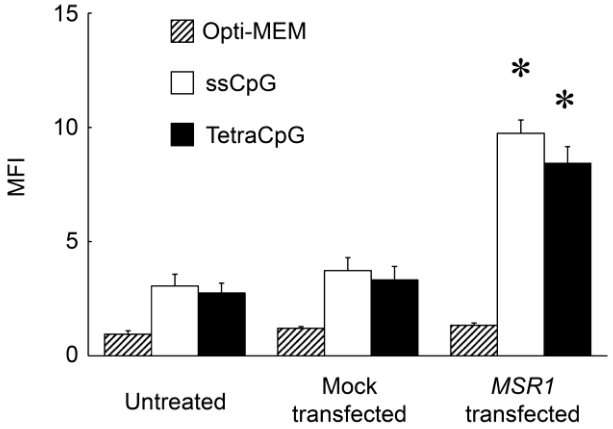

Figure 37. Uptake of ssCpG and tetraCpG in untreated, mock-transfected, or *MSR1*-transfected HEK-Blue hTLR9 cells. Each Alexa Fluor 488-labeled DNA sample was added to cells at a concentration of 2 μg/mL. The results are expressed as means + SEM of three independent experiments. **P* < 0.05 compared with the mock-transfected group.

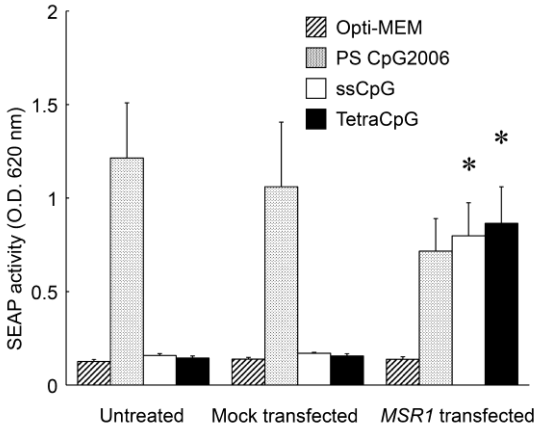

Figure 38. Secreted embryonic alkaline phosphatase (SEAP) release from untreated, mock-transfected, or *MSR1*-transfected HEK-Blue hTLR9 cells using HEK-Blue detection solution. Each DNA sample was added to the cells at a final concentration of 50 μg/mL, and the OD of the sample was measured at 620 nm. All oligodeoxynucleotides (ODNs) have a phosphodiester backbone except for CpG2006. The results are expressed as means + SEM of three independent experiments. **P* < 0.05 compared with the mock-transfected group.

The uptake of Alexa Fluor 488-ssCpG and tetraCpG was examined in the presence of anti-hMSR1 antibody to confirm the involvement of hMSR1 in the uptake of DNA by HEK-Blue hTLR9/hMSR1 cells. Figure 39 shows the MFI of mock-transfected HEK-Blue hTLR9 cells and HEK-Blue hTLR9/hMSR1 cells after the addition of Alexa Fluor 488-labeled DNA samples in the presence of hMSR1 antibody or murine IgG1 isotype control antibody. Anti-hMSR1 antibody significantly reduced the uptake of Alexa Fluor 488-ssCpG and tetraCpG in the HEK-Blue hTLR9/hMSR1 cells.

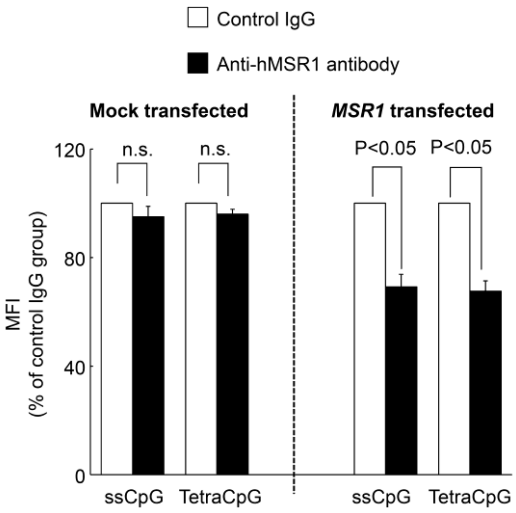

Figure 39. Cellular uptake of ssCpG and tetraCpG in mock-transfected or *MSR1*-transfected HEK-Blue hTLR9 cells in the presence of mouse IgG1 isotype control or hMSR1 antibody. Each Alexa Fluor 488-labeled DNA sample was added to cells at a final concentration of 2 μg/mL. The results are expressed as means + SEM of four independent experiments.

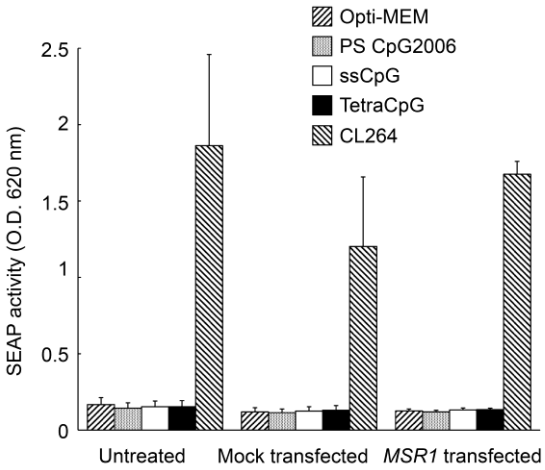

Figure 40. Secreted embryonic alkaline phosphatase (SEAP) release from untreated, mock-transfected, or *MSR1*-transfected HEK-Blue hTLR7 cells using a HEK-Blue detection solution. Each DNA sample was added to the cells at a final concentration of 50 μg/mL. The sample optical density (OD) was measured at 620 nm. The results are expressed as means + SEM of three independent experiments. CL264; a TLR7 ligand.

III-3-c. Experiments using HEK-Blue hTLR7 cells

To exclude the possibility that the expression of hMSR1 results in SEAP release without recognition of CpG DNA by TLR9, HEK-Blue hTLR7 cells were used instead of HEK-Blue hTLR9. The expression of hMSR1 in HEK-Blue hTLR7/hMSR1 cells was confirmed by western blotting (data not shown). Figure 40 shows SEAP activity after the addition of PS CpG2006, ssCpG, and tetraCpG to HEK-Blue hTLR7 cells. CL264, a TLR7 ligand, induced significant SEAP release. In contrast, PS CpG2006, ssCpG, and tetraCpG scarcely induced SEAP release from the HEK-Blue hTLR7 cells, irrespective of the expression of hMSR1. These results indicate that SEAP is released from HEK-Blue hTLR9/hMSR1 cells through the recognition of CpG DNA by TLR9.

III-4 Discussion

In the present study, I demonstrated that HEK-Blue hTLR9 cells efficiently responded to PS CpG DNA, which has high binding affinity for cell membranes, whereas they hardly responded to natural, PO CpG DNA, in spite of the fact that the cells expressed human TLR9. I also found that the low cellular uptake of PO CpG DNA by HEK-Blue hTLR9 cells explains their limited response to PO CpG DNA, and that transformation of the cells with a plasmid expressing hMSR1, a DNA receptor, restored the response of the cells to PO CpG DNA. Therefore, HEK-Blue hTLR9/hMSR1 cells can be used as a sensitive screening system for compounds that activate TLR9, although it could be difficult using HEK-Blue hTLR9/hMSR1 cells to discuss the physiological processes of the interaction of CpG DNA with TLR9-expressing cells or the mechanistic details of the cellular uptake of DNA.

The results of the present study suggest that hMSR1 or other DNA receptors are expressed in HEK-Blue hTLR9 or HEK293 cells. HEK293 cells, the parental cell line of HEK-Blue hTLR9 cells, have been widely used for the transfection of genes because they facilitate easy transformation. Therefore, HEK-Blue hTLR9 cells are also suitable for transfection studies. Both HEK293 cells and HEK-Blue hTLR9 cells hardly take up PO DNA, so they can be used to explore the receptors responsible for DNA binding, especially PO DNA binding.

MSR1 is a membrane protein that is located on the cell surface of macrophages and dendritic cells[96,97]. I found that the hMSR1 expressed in HEK-Blue hTLR9/hMSR1 cells also localized at the cell membrane (Figure 35B). The MSR1 cDNA used in the present study contained hMSR1 signal-anchor sequences, so it is reasonable to assume that hMSR1 is appropriately sorted to the correct destination (the cell membrane). It has been reported that ligation to MSR1 induces clathrin-mediated endocytosis, and that the ligands are then sorted to endosomes[98]. The mechanistic details of the uptake of DNA by HEK-Blue hTLR9/hMSR1 cells were not investigated in this study, but the efficient response to PO CpG DNA strongly suggests that the cells take up DNA in a similar manner to that adopted by other types of cells that express MSR1, such as dendritic cells.

Several reports suggest that hMSR1 is involved in the cellular uptake of PS CpG DNA[99]. However, the present study demonstrated that hMSR-1 expression had no significant effect on the cellular uptake of Alexa Fluor 488-PS CpG DNA (data not shown) or on SEAP release (Figure 38). PS CpG DNA binds strongly to cell surfaces[100], and would mask any hMSR1-mediated cellular uptake of PS CpG DNA, even if it occurred.

Although most TLR9 is found in the endosomes, TLR9 is also detected on the surface of cells in some cell types[101,102]. Some reports discussed that the cell surface TLR9 promoted the cellular uptake of CpG DNA as well as CpG DNA-coupled siRNA[103–105]. In these studies, PS CpG DNA and the antisense strand of siRNA were conjugated and, therefore, strong binding of PS CpG DNA to the cell surface could lead to efficient uptake of the conjugate. Zhang et al. demonstrated that the cell surface TLR9 did not participate in the uptake of CpG DNA[104]. Therefore, the cell surface TLR9 on HEK-Blue hTLR9/hMSR1 cells, even if it exists, would not be critical for the immune responses to PO CpG DNA.

Previous studies from my laboratory demonstrated that in RAW264.7, DC2.4, and bone marrow-derived dendritic cells (BMDCs) nanostructured DNAs were taken up more efficiently than single-stranded or double-stranded DNAs[24,25,38,44,56]. In the present study, I showed that hMSR1 can recognize nanostructured DNAs, such as tetrapodna. However, no significant differences were observed in the uptake by HEK-Blue hTLR9/hMSR1 cells between Alexa Fluor 488-ssCpG and Alexa Fluor 488-tetraCpG. These differences suggest that cell surface receptors other than MSR1 or auxiliary molecules are involved in the efficient cellular uptake of DNAs with complicated structures.

Taken together, the results of the present chapter demonstrate that the reconstruction of toll-like receptor 9-mediated responses to CpG DNA in HEK-Blue hTLR9 cells is useful for evaluating and predicting the TLR9-dependent toxicity of nucleic acid drug candidates, irrespective of their physicochemical properties. My results also suggest that the combination of HEK-Blue hTLR9 cells and natural PO CpG DNA can be used to

screen DNA receptors or DNA-binding proteins on the cell surface. Additional studies on other cell surface DNA receptors will improve understanding of the mechanisms underlying the interactions between DNA and cells at the molecular level[106].

Summary

Recently, DNA nanotechnology has attracted attention because of their ease of design. Many researchers including my laboratory reported that nanostructured DNA could be used for drug loading. However, there are little information about their delivery strategies, and is no report about the detail of the interaction of nanostructured DNA with immune cells. Nucleic acid drugs including CpG DNA need to be efficiently delivered to immune cells.

In this thesis, to clarify the characteristics of nanostructured DNA for efficient uptake of nucleic acid drugs by immune cells, I designed three big chapters.

In Chapter I, I aimed to elucidate the structural properties of nanostructured DNA to interact with immune cells. My laboratory previously reported that polypod-like structured DNA is useful for delivery of CpG DNA to immune cells such as macrophages or dendritic cells. Other group also reported that tetrahedral DNA could improve immune response from immune cells by CpG DNA. To clarify the structural property for efficient delivery, I elucidated immune response and physical properties using tetrapodna, tetrahedron, and tetragon. Then, a correlation was obtained between the structural properties and cellular uptake of nanostructured DNA. Moreover, I also revealed that nanostructured DNAs were more efficiently taken up by immune cells than by non-immune cells.

In Chapter II, I focused on structural rigidity and structural compactness of nanostructured DNA. To examine the effect of structural flexibility of DNA on their interaction with immune cells, I used DNA origami technology. Then, rectangular DNAs with many staples, more rigid structure, were efficiently interaction with RAW264.7 cells. Also, I elucidated using rolling circular amplification. More compact structure using cholesterol modified DNA was efficiently taken up by RAW264.7 cells.

In Chapter III, I tried to identify the cell surface receptor of nanostructured DNA. There are several reports about cell surface receptors of DNA, however their contribution to uptake of nanostructured DNA has not been fully elucidated. I elucidated their receptors transfected to HEK-Blue hTLR9 cells. I obtained the finding that scavenger receptor MSR1 is the cell surface receptor that recognizes nanostructured DNA.

In conclusion of my thesis, structural rigidity of nanostructured DNA is a key for their interaction with immune cells through cell surface receptors including MSR1.

Acknowledgements

I would like to express my sincere gratitude and thanks to Dr. Yoshinobu Takakura, Professor of Department of Biopharmaceutics and Drug Metabolism, Graduate School of Pharmaceutical Sciences, Kyoto University, Japan for giving me wonderful opportunities and their support with his patience, motivation, enthusiasm, and immense knowledge. His guidance helped me in all the time of research and writing of this thesis.

I am extremely grateful to my research guides, Dr. Makiya Nishikawa, Professor of Laboratory of Biopharmaceutics, Faculty of Pharmaceutical Sciences, Tokyo University of Science, Japan. It was a great opportunity to do my doctoral program under his guidance and to learn from his research expertise in Department of Biopharmaceutics and Drug Metabolism, Graduate School of Pharmaceutical Sciences, Kyoto University, Japan. All of his encouragements, insightful comments, and hard questions are fully helpful and essential for my Ph.D. course.

I wish to express my deepest appreciation to Dr. Yuki Takahashi, Associate Professor of Department of Biopharmaceutics and Drug Metabolism, Kyoto University, Japan for his patient supervision, insightful comments, suggestions, guidance and direction, valuable discussions and supports facilitating the successful completion of this study throughout the whole this study.

I highly appreciate the supports received through the collaborative work provided from Dr. Hiroshi Sugiyama, Professor of Institute for Integrated Cell-Material Sciences (iCeMS), Kyoto University, Japan, and Department of Chemistry, Graduate School of Science, Kyoto University, Japan; Dr. Masayuki Endo, Associate Professor of Institute for Integrated Cell-Material Sciences (iCeMS), Kyoto University, Japan. They kindly supported on data collection by Atomic force microscopy in Chapter I and Chapter II.

I also express my sincere appreciations to collaborative works provided from Dr. Norimitsu Kadowaki, Professor of Department of Internal Medicine, Faculty of Medicine, Kagawa University, Japan and Dr. Kenichi Ishiyama. They worked altogether with me in isolation of human PBMCs in Chapter I.

I would like to express my appreciations to collaborative works from Dr. Shinji Sakuma, Professor of Laboratory of Drug Delivery System, Faculty of Pharmaceutical Sciences, Setsunan University, Japan. He worked altogether with me in Section 3 of Chapter I.

I appreciate profoundly to Dr. Takao Inoue, Division of Molecular Target and Gene Therapy Products, National Institute of Health Sciences, Japan for his kind gift of HEK-Blue TLR cells and helpful guidance and discussions in Chapter III.

I also express my sincere appreciations to collaborative works provided from Dr. Mireille Lahoud, Associate Professor of Department of Biochemistry and Molecular Biology, Monash University, Australia. DEC-205 plasmid was kindly provided by her.

I would like to express sincere gratitude to Dr. Kohta Mohri, Mr. Noriyuki Matsuzaki, Ms. Yukako Shiba, Ms. Kanako Sugimura, Mr. Keisuke Umemura, Mr. Tatsuoki Maezawa, and Ms. Mutsumi Kariya for their great achievement and contribution as a co-author for my thesis, and their advice and warm support for this study.

I am greatly indebted to all members of Department of Biopharmaceutics and Drug metabolism and of Drug Delivery Research, Graduate School of Pharmaceutics Sciences, Kyoto University for their experimental assistance.

Finally, I would like to express my deepest gratitude to all of my family for their support, encouragements, and understanding throughout the doctoral course of this study.

List of Publications

Optimal arrangement of four short DNA strands for delivery of immunostimulatory nucleic acids to immune cells.

Shozo Ohtsuki, Noriyuki Matsuzaki, Kohta Mohri, Masayuki Endo, Tomoko Emura, Kumi Hidaka, Hiroshi Sugiyama, Yuki Takahashi, Kenichi Ishiyama, Norimitsu Kadowaki, Yoshinobu Takakura, Makiya Nishikawa.

Nucleic Acid Therapeutics **25**, 245-253 (2015).

Effect of the structural properties of tripod-like structured DNA on their interaction with macrophage-like RAW264.7 cells.

Shozo Ohtsuki, Yuki Takahashi, Yoshinobu Takakura, Makiya Nishikawa.

Manuscript in preparation

Elucidation of the mechanism of increased activity of immunostimulatory DNA by the formation of polypod-like structure.

Kohta Mohri, Kengo Nagata, Shozo Ohtsuki, Shiori Toyama, Mao Nonomura, Yuki Takahashi, Yoshinobu Takakura, Makiya Nishikawa, Shinji Sakuma.

Pharmaceutical Research **34**, 2362-2370 (2017).

Folding of single-stranded circular DNA into rigid rectangular DNA origami accelerates its cellular uptake.

Shozo Ohtsuki, Yukako Shiba, Tatsuoki Maezawa, Yuki Takahashi, Masayuki Endo, Tomoko Emura, Kumi Hidaka, Hiroshi Sugiyama, Yoshinobu Takakura, Makiya Nishikawa.

Manuscript in preparation

Development of DNA supramolecules formed by hydrophobic interaction for the effective delivery of CpG DNA.

Shozo Ohtsuki, Kanako Sugimura, Yuki Takahashi, Mutsumi Kariya, Makiya Nishikawa, Yoshinobu Takakura.

Manuscript in preparation

Reconstruction of Toll-like receptor 9-mediated response to CpG DNA in HEK-Blue hTLR9 cells by transfection of human macrophage scavenger receptor 1 gene.

Shozo Ohtsuki, Yuki Takahashi, Takao Inoue, Yoshinobu Takakura, Makiya Nishikawa.

Scientific Reports **7**, 13661 (2017).

Other Publications

Self-assembling DNA dendrimer for effective delivery of immunostimulatory CpG DNA to immune cells.

Kohta Mohri, Eri Kusuki, Shozo Ohtsuki, Natsuki Takahashi, Masayuki Endo, Kumi Hidaka, Hiroshi Sugiyama, Yuki Takahashi, Yoshinobu Takakura, Makiya Nishikawa.

Biomacromolecules **16**, 1095-1101 (2015).

Self-assembling DNA hydrogel-based delivery of immunoinhibitory nucleic acids to immune cells.

Yu Nishida, Shozo Ohtsuki, Yuki Araie, Yuka Umeki, Masayuki Endo, Tomoko Emura, Kumi Hidaka, Hiroshi Sugiyama, Yuki Takahashi, Yoshinobu Takakura, Makiya Nishikawa.

Nanomedicine **12**, 123-130 (2016).

DNA nanotechnology-based composite-type gold nanoparticle-immunostimulatory DNA hydrogel for tumor photothermal immunotherapy.

Tomoya Yata, Yuki Takahashi, Mengmeng Tan, Hirotaka Nakatsuji, Shozo Ohtsuki, Tatsuya Murakami, Hiroshi Imahori, Yuka Umeki, Tomoki Shiomi, Yoshinobu Takakura, Makiya Nishikawa.

Biomaterials **146**, 136-145 (2017).

References

1. Fattal, E. and Bochot, A. Ocular delivery of nucleic acids: antisense oligonucleotides, aptamers and siRNA. *Adv. Drug Deliv. Rev.* **58,** 1203–1223 (2006).
2. Dove, A. Antisense and sensibility. *Nat. Biotechnol.* **20,** 121–124 (2002).
3. Chen, C., Yang, Z. and Tang, X. Chemical modifications of nucleic acid drugs and their delivery systems for gene-based therapy. *Med. Res. Rev.* 1–41 (2018).
4. Khvorova, A. and Watts, J. K. The chemical evolution of oligonucleotide therapies of clinical utility. *Nat. Biotechnol.* **35,** 238–248 (2017).
5. Kanasty, R., Dorkin, J. R., Vegas, A. and Anderson, D. Delivery materials for siRNA therapeutics. *Nat. Mater.* **12,** 967–977 (2013).
6. Khorkova, O. and Wahlestedt, C. Oligonucleotide therapies for disorders of the nervous system. *Nat. Biotechnol.* **35,** 249–263 (2017).
7. Hemmi, H., Takeuchi, O., Kawai, T., Kaisho, T., Sato, S., Sanjo, H., Matsumoto, M., Hoshino, K., Wagner, H., Takeda, K. and Akira, S. A Toll-like receptor recognizes bacterial DNA A Toll-like receptor recognizes bacterial DNA. *Nature* **408,** 740–745 (2000).
8. Klinman, D. M., Yi, A. K., Beaucage, S. L., Conover, J. and Krieg, A. M. CpG motifs present in bacteria DNA rapidly induce lymphocytes to secrete interleukin 6, interleukin 12, and interferon gamma. *Proc. Natl. Acad. Sci. U. S. A.* **93,** 2879–83 (1996).
9. Krug, A., Rothenfusser, S., Hornung, V., Jahrsdrfer, B., Blackwell, S., Ballas, Z. K., Endres, S., Krieg, A. M. and Hartmann, G. Identification of CpG oligonucleotide sequences with high induction of IFN-α/β in plasmacytoid dendritic cells. *Eur. J. Immunol.* **31,** 2154–2163 (2001).
10. Wagner, H. Toll meets bacterial CpG-DNA. *Immunity* **14,** 499–502 (2001).
11. Krieg, A. M. CpG motifs in bacterial DNA and their immune effects. *Annu Rev Immunol.* **20,** 709–760 (2002).
12. Klinman, D. M. Immunotherapeutic uses of CpG oligodeoxynucleotides. *Nat. Rev. Immunol.* **4,** 249–259 (2004).
13. Krieg, A. M. Therapeutic potential of toll-like receptor 9 activation. *Nat. Rev. Drug Discov.* **5,** 471–484 (2006).
14. Vollmer, J. and Krieg, A. M. Immunotherapeutic applications of CpG oligodeoxynucleotide TLR9 agonists. *Adv. Drug Deliv. Rev.* **61,** 195–204 (2009).
15. Kawai, T. and Akira, S. Toll-like Receptors and Their Crosstalk with Other Innate Receptors in Infection and Immunity. *Immunity* **34,** 637–650 (2011).
16. Gupta, G. K. and Agrawal, D. K. CpG Oligodeoxynucleotides as TLR9 Agonists. **24,** 225–235 (2010).
17. Rothemund, P. W. K. Folding DNA to create nanoscale shapes and patterns. *Nature* **440,** 297–302 (2006).
18. Zhang, C., Su, M., He, Y., Zhao, X., Fang, P., Ribbe, A. E., Jiang, W. and Mao, C. Conformational flexibility facilitates self-assembly of complex DNA nanostructures. *Proc. Natl. Acad. Sci. U. S. A.* **105,** 10665–10669

(2008).

19. He, Y., Ye, T., Su, M., Zhang, C., Ribbe, A. E., Jiang, W. and Mao, C. Hierarchical self-assembly of DNA into symmetric supramolecular polyhedra. *Nature* **452,** 198–201 (2008).
20. Um, S. H., Lee, J. B., Park, N., Kwon, S. Y., Umbach, C. C. and Luo, D. Enzyme-catalysed assembly of DNA hydrogel. *Nat. Mater.* **5,** 797–801 (2006).
21. Schmidt, T. L. and Heckel, A. Construction of a structurally defined double-stranded DNA catenane. *Nano Lett.* **11,** 1739–1742 (2011).
22. Nishikawa, M., Matono, M., Rattanakiat, S., Matsuoka, N. and Takakura, Y. Enhanced immunostimulatory activity of oligodeoxynucleotides by Y-shape formation. *Immunology* **124,** 247–255 (2008).
23. Nishikawa, M., Mizuno, Y., Mohri, K., Matsuoka, N., Rattanakiat, S., Takahashi, Y., Funabashi, H., Luo, D. and Takakura, Y. Biodegradable CpG DNA hydrogels for sustained delivery of doxorubicin and immunostimulatory signals in tumor-bearing mice. *Biomaterials* **32,** 488–494 (2011).
24. Mohri, K., Nishikawa, M., Takahashi, N., Shiomi, T., Matsuoka, N., Ogawa, K., Endo, M., Hidaka, K., Sugiyama, H., Takahashi, Y. and Takakura, Y. Design and development of nanosized DNA assemblies in polypod-like structures as efficient vehicles for immunostimulatory cpg motifs to immune cells. *ACS Nano* **6,** 5931–5940 (2012).
25. Uno, S., Nishikawa, M., Mohri, K., Umeki, Y., Matsuzaki, N., Takahashi, Y., Fujita, H., Kadowaki, N. and Takakura, Y. Efficient delivery of immunostimulatory DNA to mouse and human immune cells through the construction of polypod-like structured DNA. *Nanomedicine Nanotechnology, Biol. Med.* **10,** 765–774 (2014).
26. Li, J., Fan, C., Pei, H., Shi, J. and Huang, Q. Smart drug delivery nanocarriers with self-assembled DNA nanostructures. *Adv. Mater.* **25,** 4386–4396 (2013).
27. Nishikawa, M., Ogawa, K., Umeki, Y., Mohri, K., Kawasaki, Y., Watanabe, H., Takahashi, N., Kusuki, E., Takahashi, R., Takahashi, Y. and Takakura, Y. Injectable, self-gelling, biodegradable, and immunomodulatory DNA hydrogel for antigen delivery. *J. Control. Release* **180,** 25–32 (2014).
28. Nishikawa, M., Rattanakiat, S. and Takakura, Y. DNA-based nano-sized systems for pharmaceutical and biomedical applications. *Adv. Drug Deliv. Rev.* **62,** 626–632 (2010).
29. Matsuoka, N., Nishikawa, M., Mohri, K., Rattanakiat, S. and Takakura, Y. Structural and immunostimulatory properties of Y-shaped DNA consisting of phosphodiester and phosphorothioate oligodeoxynucleotides. *J. Control. Release* **148,** 311–316 (2010).
30. Hancock, R. E. W., Nijnik, A. and Philpott, D. J. Modulating immunity as a therapy for bacterial infections. *Nat. Rev. Microbiol.* **10,** 243–254 (2012).
31. O'Neill, L. A. J., Hennessy, E. J. and Parker, A. E. Targeting Toll-like receptors: Emerging therapeutics? *Nat. Rev. Drug Discov.* **9,** 293–307 (2010).
32. Li, J., Pei, H., Zhu, B., Liang, L., Wei, M., He, Y., Chen, N., Li, D., Huang, Q. and Fan, C. Self-assembled multivalent DNA nanostructures for noninvasive intracellular delivery of immunostimulatory CpG

oligonucleotides. *ACS Nano* **5,** 8783–8789 (2011).

33. Kawamura, K., Kadowaki, N., Kitawaki, T. and Uchiyama, T. Virus-stimulated plasmacytoid dendritic cells induce CD4 ♀ cytotoxic regulatory T cells. *Control* **107,** 1031–1038 (2006).
34. Endo, M., Katsuda, Y., Hidaka, K. and Sugiyama, H. Regulation of DNA methylation using different tensions of double strands constructed in a defined DNA nanostructure. *J. Am. Chem. Soc.* **132,** 1592–1597 (2010).
35. Benimetskaya, L., Loike, J. D., Khaled, Z., Loike, G., Silverstein, S. C., Cao, L., El Khoury, J., Cai, T. Q. and Stein, C. A. Mac-1 (CD11b/CD18) is an oligodeoxynucleotide-binding protein. *Nat. Med.* **3,** 414–420 (1997).
36. Siess, D. C., Vedder, C. T., Merkens, L. S., Tanaka, T., Freed, A. C., McCoy, S. L., Heinrich, M. C., Deffebach, M. E., Bennett, R. M. and Hefeneider, S. H. A human gene coding for a membrane-associated nucleic acid-binding protein. *J. Biol. Chem.* **275,** 33655–33662 (2000).
37. Tversky, J. R., Le, T. V., Bieneman, A. P., Chichester, K. L., Hamilton, R. G. and Schroeder, J. T. Human blood dendritic cells from allergic subjects have impaired capacity to produce interferon-α via toll-like receptor 9. *Clin. Exp. Allergy* **38,** 781–788 (2008).
38. Ohtsuki, S., Matsuzaki, N., Mohri, K., Endo, M., Emura, T., Hidaka, K., Sugiyama, H., Takahashi, Y., Ishiyama, K., Kadowaki, N., Takakura, Y. and Nishikawa, M. Optimal Arrangement of Four Short DNA Strands for Delivery of Immunostimulatory Nucleic Acids to Immune Cells. *Nucleic Acid Ther.* **25,** 245–53 (2015).
39. Chithrani, B. D., Ghazani, A. A. and Chan, W. C. W. Determining the size and shape dependence of gold nanoparticle uptake into mammalian cells. *Nano Lett.* **6,** 662–668 (2006).
40. He, C., Hu, Y., Yin, L., Tang, C. and Yin, C. Effects of particle size and surface charge on cellular uptake and biodistribution of polymeric nanoparticles. *Biomaterials* **31,** 3657–3666 (2010).
41. Yin Win, K. and Feng, S. S. Effects of particle size and surface coating on cellular uptake of polymeric nanoparticles for oral delivery of anticancer drugs. *Biomaterials* **26,** 2713–2722 (2005).
42. Zhong, M. and Kallenbach, N. R. Conformation and Thermodynamics of DNA 'Necks'; Models for Three-arm Branch Formation in a Duplex. *Journal of molecular biology* **230,** 766–778 (1993).
43. Platt, N., Suzukit, H., Kuriharat, Y., Kodamat, T., Gordon, S. and Steinberg, D. Role for the class A macrophage scavenger receptor in the phagocytosis of apoptotic thymocytes in vitro. *Immunology* **93,** 12456–12460 (1996).
44. Nishida, Y., Ohtsuki, S., Araie, Y., Umeki, Y., Endo, M., Emura, T., Hidaka, K., Sugiyama, H., Takahashi, Y., Takakura, Y. and Nishikawa, M. Self-assembling DNA hydrogel-based delivery of immunoinhibitory nucleic acids to immune cells. *Nanomedicine Nanotechnology, Biol. Med.* **12,** 123–130 (2016).
45. Swanson, J. a and Watts, C. Macropinocytosis. *Trends Cell Biol.* **5,** 424–428 (1995).
46. Swanson, J. A. Shaping cups into phagosomes and macropinosomes. *Nat. Rev. Mol. Cell Biol.* **9,** 639–649 (2008).
47. Conner, S. D. and Schmid, S. L. Regulated portals of entry into the cell. *Nature* **422,** 37–44 (2003).
48. Doherty, G. J. and McMahon, H. T. Mechanisms of Endocytosis. *Annu. Rev. Biochem.* **78,** 857–902 (2009).

49. Oh, N. and Park, J. H. Endocytosis and exocytosis of nanoparticles in mammalian cells. *Int. J. Nanomedicine* **9,** 51–63 (2014).

50. Seeman, N. C. DNA in a material world. *50 Years DNA* **421,** 113–117 (2016).

51. Seeman, N. C. Nucleic acid junctions and lattices. *J. Theor. Biol.* **99,** 237–247 (1982).

52. Liedl, T., Högberg, B., Tytell, J., Ingber, D. E. and Shih, W. M. Self-assembly of three-dimensional prestressed tensegrity structures from DNA. *Nat. Nanotechnol.* **5,** 520–524 (2010).

53. Andersen, E. S., Dong, M., Nielsen, M. M., Jahn, K., Subramani, R., Mamdouh, W., Golas, M. M., Sander, B., Stark, H., Oliveira, C. L. P., Pedersen, J. S., Birkedal, V., Besenbacher, F., Gothelf, K. V. and Kjems, J. Self-assembly of a nanoscale DNA box with a controllable lid. *Nature* **459,** 73–76 (2009).

54. Subramanian, H. K. K., Chakraborty, B., Sha, R. and Seeman, N. C. The Label-Free Unambiguous Detection and Symbolic Display of Single Nucleotide Polymorphisms on DNA Origami. 910–913 (2011).

55. Movshovich, R., Vekhter, I., Pagliuso, P. G., Sarrao, J. L., Paglione, J., Taillefer, L., Ovchinnikov, Y. N., Ferrell, R. A., Shimahara, H., Movshovich, R., Capan, C., Pagliuso, P. G., Sarrao, J. L., Dewhurst, C. D., Hoogenboom, B. W., Canfield, P. C., Dewhurst, C. D., Hoogenboom, B. W., Eskildsen, M. R., *et al.* Self-Assembled Water-Soluble Nucleic Acid Probe Tiles for Label-Free RNA Hybridization Assays. 180–184 (2008).

56. Mohri, K., Kusuki, E., Ohtsuki, S., Takahashi, N., Endo, M., Hidaka, K., Sugiyama, H., Takahashi, Y., Takakura, Y. and Nishikawa, M. Self-Assembling DNA Dendrimer for Effective Delivery of Immunostimulatory CpG DNA to Immune Cells. *Biomacromolecules* **16,** 1095–1101 (2015).

57. Umeki, Y., Mohri, K., Kawasaki, Y., Watanabe, H. and Takahashi, R. Induction of Potent Antitumor Immunity by Sustained Release of Cationic Antigen from a DNA-Based Hydrogel with Adjuvant Activity. 5758–5767 (2015).

58. Yata, T., Takahashi, Y., Tan, M., Nakatsuji, H., Ohtsuki, S., Murakami, T., Imahori, H., Umeki, Y., Shiomi, T., Takakura, Y. and Nishikawa, M. DNA nanotechnology-based composite-type gold nanoparticle-immunostimulatory DNA hydrogel for tumor photothermal immunotherapy. *Biomaterials* **146,** 136–145 (2017).

59. Erkelenz, M., Bauer, D. M., Meyer, R., Gatsogiannis, C., Raunser, S., Saccà, B. and Niemeyer, C. M. A facile method for preparation of tailored scaffolds for DNA-origami. *Small* **10,** 73–77 (2014).

60. Pound, E., Ashton, J. R., Becerril, H. A. and Woolley, A. T. Polymerase chain reaction based scaffold preparation for the production of thin, branched DNA origami nanostructures of arbitrary sizes. *Nano Lett.* **9,** 4302–4305 (2009).

61. Petros, R. A. and Desimone, J. M. Strategies in the design of nanoparticles for therapeutic applications. *Nat. Rev. Drug Discov.* **9,** 615–627 (2010).

62. Lombardo, D., Kiselev, M. A., Magazù, S. and Calandra, P. Amphiphiles Self-Assembly : Basic Concepts and Future Perspectives of Supramolecular Approaches. **2015,** (2015).

63. Liechty, W. B., Kryscio, D. R., Slaughter, B. V and Peppas, N. A. Polymers for Drug Delivery Systems. *Annu Rev Chem Biomol Eng.* **1,** 149–173 (2010).

64. Singh, R. S., Saini, G. K. and Kennedy, J. F. Pullulan : Microbial sources , production and applications. *Carbohydr Polym.* **73,** 515–531 (2008).

65. Kazunari Akiyoshi, Shigeru Deguchi, Nobuhiro Moriguchi, Shigehiko Yamaguchi, J. S. Self-Aggregates of Hydrophobized Polysaccharides in Water. Formation and Characteristics of Nanoparticles. *Macromolecules* **26,** 3062–3068 (1993).

66. Akiyoshi, K., Kobayashi, S., Shichibe, S., Mix, D., Baudys, M., Kim, S. W. and Sunamoto, J. Self-assembled hydrogel nanoparticle of cholesterol-bearing pullulan as a carrier of protein drugs : Complexation and stabilization of insulin. *J Control Release.* **54,** 313–320 (1998).

67. Vinogradov, S. V, Batrakova, E. V and Kabanov, A. V. Nanogels for Oligonucleotide Delivery to the Brain. *Bioconjug Chem.* **15,** 50–60 (2004).

68. Fire, A. and Xu, S. Q. Rolling replication of short DNA circles. *Proc. Natl. Acad. Sci.* **92,** 4641–4645 (1995).

69. Liu, D., Daubendiek, S. L., Zillman, M. A., Ryan, K. and Kool, E. T. Rolling circle DNA synthesis: Small circular oligonucleotides as afficient templates for DNA polymerases. *J Am Chem Soc* **118,** 1587–1594 (1996).

70. Chono, S., Tanino, T., Seki, T. and Morimoto, K. Uptake characteristics of liposomes by rat alveolar macrophages: influence of particle size and surface mannose modification. *J. Pharm. Pharmacol.* **59,** 75–80 (2007).

71. Champion, J. A. and Mitragotri, S. Shape induced inhibition of phagocytosis of polymer particles. *Pharm. Res.* **26,** 244–249 (2009).

72. Ali, M. M., Li, F., Zhang, Z., Zhang, K., Kang, D.-K., Ankrum, J. A., Le, X. C. and Zhao, W. Rolling circle amplification: a versatile tool for chemical biology, materials science and medicine. *Chem. Soc. Rev.* **43,** 3324–3341 (2014).

73. Weiner, G. J., Liu, H.-M., Wooldridge, J. E., Dahle, C. E. and Krieg, A. M. Immunostimulatory oligodeoxynucleotides containing the CpG motif are effective as immune adjuvants in tumor antigen immunization. *Proc. Natl. Acad. Sci.* **94,** 10833–10837 (1997).

74. Liu, X., Xu, Y., Yu, T., Clifford, C., Liu, Y., Yan, H. and Chang, Y. A DNA nanostructure platform for directed assembly of synthetic vaccines. *Nano Lett.* **12,** 4254–4259 (2012).

75. Krishnamachari, Y. and Salem, A. K. Innovative strategies for co-delivering antigens and CpG oligonucleotides. *Adv. Drug Deliv. Rev.* **61,** 205–217 (2009).

76. Yoshikawa, T., Okada, N., Oda, A., Matsuo, K., Matsuo, K., Kayamuro, H., Ishii, Y., Yoshinaga, T., Akagi, T., Akashi, M. and Nakagawa, S. Nanoparticles built by self-assembly of amphiphilic gamma-PGA can deliver antigens to antigen-presenting cells with high efficiency: a new tumor-vaccine carrier for eliciting effector T cells. *Vaccine* **26,** 1303–1313 (2008).

77. Gu, X., Schmitt, M., Hiasa, A., Nagata, Y., Ikeda, H., Sasaki, Y., Akiyoshi, K., Smininolo, J., Nakamura, H.,

Kuribayashi, K. and Shiku, H. A Novel Hydrophobized Polysaccharide / Oncoprotein Complex Vaccine Induces in Vitro and in Vivo Cellular and Humoral Immune Responses against HER2-expressing Murine Sarcomas. *Cancer Res.* **58,** 3385–3390 (1998).

78. Cavagnaro Joy, Berman Cindy, Kornbrust Doug, White Tacey, Campion Sarah, and H. S. Considerations for Assessment of Reproductive and Developmental Toxicity of Oligonucleotide-Based Therapeutics. *Nucleic Acid Ther.* **24,** 313–325 (2014).

79. Kleinman, M. E., Yamada, K., Takeda, A., Chandrasekaran, V., Nozaki, M., Baffi, J. Z., Albuquerque, R. J. C., Yamasaki, S., Itaya, M., Pan, Y., Appukuttan, B., Gibbs, D., Yang, Z., Karikó, K., Ambati, B. K., Wilgus, T. A., DiPietro, L. A., Sakurai, E., Zhang, K., *et al.* Sequence- and target-independent angiogenesis suppression by siRNA via TLR3. *Nature* **452,** 591–597 (2008).

80. Kariko, K., Bhuyan, P., Capodici, J. and Weissman, D. Small Interfering RNAs Mediate Sequence-Independent Gene Suppression and Induce Immune Activation by Signaling through Toll-Like Receptor 3. *J. Immunol.* **172,** 6545–6549 (2004).

81. Hornung, V., Guenthner-Biller, M., Bourquin, C., Ablasser, A., Schlee, M., Uematsu, S., Noronha, A., Manoharan, M., Akira, S., De Fougerolles, A., Endres, S. and Hartmann, G. Sequence-specific potent induction of IFN-α by short interfering RNA in plasmacytoid dendritic cells through TLR7. *Nat. Med.* **11,** 263–270 (2005).

82. Judge, A. D., Sood, V., Shaw, J. R., Fang, D., McClintock, K. and MacLachlan, I. Sequence-dependent stimulation of the mammalian innate immune response by synthetic siRNA. *Nat. Biotechnol.* **23,** 457–462 (2005).

83. Marjorie Robbins, Adam Judge, and I. M. siRNA and Innate Immunity. *Oligonucleotides* **19,** 89–102 (2009).

84. Sioud, M. Induction of inflammatory cytokines and interferon responses by double-stranded and single-stranded siRNAs is sequence-dependent and requires endosomal localization. *J. Mol. Biol.* **348,** 1079–1090 (2005).

85. Sledz, C. A., Holko, M., De Veer, M. J., Silverman, R. H. and Williams, B. R. G. Activation of the interferon system by short-interfering RNAs. *Nat. Cell Biol.* **5,** 834–839 (2003).

86. Krieg, A. M. CpG motifs: The active ingredient in bacterial extracts? *Nat. Med.* **9,** 831–835 (2003).

87. Krug, A., French, A. R., Barchet, W., Fischer, J. A. A., Dzionek, A., Pingel, J. T., Orihuela, M. M., Akira, S., Yokoyama, W. M. and Colonna, M. TLR9-dependent recognition of MCMV by IPC and DC generates coordinated cytokine responses that activate antiviral NK cell function. *Immunity* **21,** 107–119 (2004).

88. Latz, E., Schoenemeyer, A., Visintin, A., Fitzgerald, K. A., Monks, B. G., Knetter, C. F., Lien, E., Nilsen, N. J., Espevik, T. and Golenbock, D. T. TLR9 signals after translocating from the ER to CpG DNA in the lysosome. *Nat. Immunol.* **5,** 190–198 (2004).

89. Rutz, M., Metzger, J., Gellert, T., Luppa, P., Lipford, G. B., Wagner, H. and Bauer, S. Toll-like receptor 9 binds single-stranded CpG-DNA in a sequence- and pH-dependent manner. *Eur. J. Immunol.* **34,** 2541–2550 (2004).

90. Kimura, Y., Sonehara, K., Kuramoto, E., Makino, T., Yamamoto, S., Yamamoto, T., Kataoka, T. and Tokunaga,

T. Binding of oligoguanylate to scavenger receptors is required for oligonucleotides to augment NK cell activity and induce IFN. *J. Biochem.* **116,** 991–994 (1994).

91. Sirois, C. M., Jin, T., Miller, A. L., Bertheloot, D., Nakamura, H., Horvath, G. L., Mian, A., Jiang, J., Schrum, J., Bossaller, L., Pelka, K., Garbi, N., Brewah, Y., Tian, J., Chang, C., Chowdhury, P. S., Sims, G. P., Kolbeck, R., Coyle, A. J., *et al.* RAGE is a nucleic acid receptor that promotes inflammatory responses to DNA. *J. Exp. Med.* **210,** 2447–2463 (2013).

92. Moseman, A. P., Moseman, E. A., Schworer, S., Smirnova, I., Volkova, T., von Andrian, U. and Poltorak, A. Mannose Receptor 1 Mediates Cellular Uptake and Endosomal Delivery of CpG-Motif Containing Oligodeoxynucleotides. *J. Immunol.* **191,** 5615–5624 (2013).

93. Caminschi, I., Meuter, S. and Heath, W. R. DEC-205 is a cell surface receptor for CpG oligonucleotides. *Oncoimmunology* **2,** (2013).

94. Nakano, T. & Yamamura, E. Patent WO2014088087 A1; PCT/JP2013/082774. (2014).

95. Haile, L. A., Puig, M., Kelley-Baker, L. and Verthelyi, D. Detection of innate immune response modulating impurities in therapeutic proteins. *PLoS One* **10,** (2015).

96. Platt, N. and Gordon, S. Scavenger receptors: diverse activities and promiscuous binding of polyanionic ligands. *Chem. Biol.* **5,** R193-203 (1998).

97. Platt, N. and Gordon, S. Is the class A macrophage scavenger receptor (SR-A) multifunctional? — The mouse ' s tale. *J. Clin. Investig.* **108,** 649–654 (2001).

98. Zani, I., Stephen, S., Mughal, N., Russell, D., Homer-Vanniasinkam, S., Wheatcroft, S. and Ponnambalam, S. Scavenger Receptor Structure and Function in Health and Disease. *Cells* **4,** 178–201 (2015).

99. Jozefowski, S. Role of scavenger receptor MARCO in macrophage responses to CpG oligodeoxynucleotides. *J. Leukoc. Biol.* **80,** 870–879 (2006).

100. Kurreck, J. Antisense technologies: Improvement through novel chemical modifications. *Eur. J. Biochem.* **270,** 1628–1644 (2003).

101. Eaton-Bassiri, A., Dillon, S. B., Cunningham, M., Rycyzyn, M. A., Mills, J., Sarisky, R. T. and Mbow, M. L. Toll-like receptor 9 can be expressed at the cell surface of distinct populations of tonsils and human peripheral blood mononuclear cells. *Infect Immun* **72,** 7202–7211 (2004).

102. Saikh, K. U., Kissner, T. L., Sultana, A., Ruthel, G. and Ulrich, R. G. Human Monocytes Infected with Yersinia pestis Express Cell Surface TLR9 and Differentiate into Dendritic Cells. *J. Immunol.* **173,** 7426–7434 (2004).

103. Nechaev, S., Gao, C., Moreira, D., Swiderski, P., Jozwiak, A., Kowolik, C. M., Zhou, J., Armstrong, B., Raubitschek, A., Rossi, J. J. and Kortylewski, M. Intracellular processing of immunostimulatory CpG-siRNA: Toll-like receptor 9 facilitates siRNA dicing and endosomal escape. *J. Control. Release* **170,** 307–315 (2013).

104. Zhang, Q., Hossain, D. S., Nechaev, S., Kozlowska, A., Zhang, W., Liu, Y., Kowolik, C. M., Swiderski, P., Rossi, J. J., Forman, S., Pal, S., Bhatia, R., Raubitschek, A., Yu, H. and Kortylewski, M. TLR9-mediated siRNA delivery for targeting of normal and malignant human hematopoietic cells in vivo. **121,** 1304–1315

(2013).

105. Kortylewski, M., Swiderski, P., Herrmann, A., Wang, L., Kowolik, C., Kujawski, M., Lee, H., Scuto, A., Liu, Y., Yang, C., Deng, J., Soifer, H. S., Raubitschek, A., Forman, S., Rossi, J. J., Pardoll, D. M., Jove, R. and Yu, H. In vivo delivery of siRNA to immune cells by conjugation to a TLR9 agonist enhances antitumor immune responses. *Nat. Biotechnol.* **27,** 925–932 (2009).

106. Ohtsuki, S., Takahashi, Y., Inoue, T., Takakura, Y. and Nishikawa, M. Reconstruction of Toll-like receptor 9-mediated responses in HEK-Blue hTLR9 cells by transfection of human macrophage scavenger receptor 1 gene. *Sci. Rep.* **7,** 13661 (2017).